Turbulence in the core

Henri-Claude Nataf, Nathanael Schaeffer

Univ. Grenoble Alpes / CNRS / IRD, ISTerre, F-38000 Grenoble, France

1. Introduction

In this chapter, we have the difficult task to describe the invisible part of the core: turbulent structures that we can't detect but have to be there... Indeed, non-linear interactions in the liquid core lead to the formation of velocity, temperature and magnetic structures on a large range of scales. Their role is important: they transfer energy between large and small length-scales, and in the end they control the dissipation of the geodynamo. Turbulence is at work everywhere and has been studied for decades. Our first step is to define turbulence and show why one should care about turbulence in the core. Then we review a few fundamental features of hydrodynamic turbulence. Many tools are needed to decipher turbulence: we present key results obtained from numerical simulations, laboratory experiments, and observations of natural systems. Unfortunately, no observations of the internal geomagnetic field are possible at small scales, mostly because of the crustal field that overprints the small-scale core field. Observations of turbulence in other systems are thus welcome, to gain insight in what could happen in the Earth's core. We also devote one section to the parametrization of turbulence in numerical simulations.

The last two sections focus on the core. Turbulence implies a range of time- and length-scales. We define dimensionless numbers depending on the length scale ℓ, that measure the relative weight of the various terms in the governing equations. Using the known properties of the core, and its large-scale velocity and magnetic field, we evaluate these various numbers. We introduce $\tau - \ell$-diagrams that help us identify the scales at which turbulent regimes change. Step by step, we explore the suite of plausible turbulent regimes for the core, introducing successively the effects of rotation and magnetic field. Our analysis emphasizes the crucial role of rotation in limiting the dissipation of the geodynamo, and points out the need for dedicated studies.

Email address: Henri-Claude.Nataf@ujf-grenoble.fr (Henri-Claude Nataf)

2. What is turbulence?

2.1. An attempt to define turbulence

Turbulence is difficult to define precisely, but we can list a few elements that characterize turbulent motion. The most prominent feature of turbulence is that the motion of the fluid involves a wide range of spatial and temporal scales. These scales cannot be treated independently and there is no scale separation between small and large scales, although different regimes can be identified.

In order for the various scales to interact, the non-linear terms of the evolution equation must be important. In the case of pure hydrodynamic turbulence, this is ensured by a large Reynolds number $\mathrm{Re} = UL/\nu \gg 1$, ratio of the diffusive time L^2/ν to the advection time L/U (L is a characteristic length, U a typical velocity, and ν the kinematic viscosity of the fluid). However, in a self-magnetized conducting fluid driven by thermo-chemical convection, there are other non-linear terms that allow interaction of different scales.

A flow executing turbulent motion often exhibits eddies of various scales, but this may not be the case when a strong magnetic field and background rotation are present, as it is the case for the Earth's core. Turbulence is not chaos, but all turbulent flows exhibit fluctuations that call for a statistical description, rather than a deterministic one. If the precise details of the flow are controlled by initial conditions or small perturbations that we cannot measure, global quantities such as the energy dissipation rate, the average velocity field, the amplitude of fluctuations are of great interest, and are expected to be well defined and measurable.

As opposed to laminar motion, where the fluid particles follow a pattern controlled by the viscosity, with

little change from one fluid particle to its neighbor, a turbulent motion involves complex time-dependence and spatial dependence.

2.2. Is the Earth's core turbulent ?

Due to the low viscosity of molten iron, the Reynolds number is certainly very large: Re $\sim 10^8$, meaning that the viscous term (which is the only isotropic dissipation term), acts mainly at small scale. Furthermore, the non-linear terms associated with the Lorentz force are in fact much larger than the inertial term at large scale, leading to a ratio of non-linear to viscous force of about 10^{12}.

However, the importance of the magnetic field and the global rotation rate make the turbulence rather peculiar. It is sometimes advocated that the flow variations along the rotation axis or magnetic field lines are inhibited, leading to sheet-like (laminar) motion which cannot be turbulent anymore (because velocity is now mostly perpendicular to its gradient). These are a lot of constraints for an incompressible vector field that has only two degrees of freedom.

We shall see in the following sections that not all these constraints have the same strength. In an attempt to describe the dynamics of the system, we will discuss how it can organize itself on a broad range of time and length-scales in several different regimes.

3. Why care?

Turbulent small-scale fields within the core will not be observed. So, why care? They can have a collective or average effect that has a direct measurable consequence on the large-scale flow and magnetic field, which we investigate. They also control the dissipation, which we need to assess in order to know how much power is needed to drive the dynamo.

3.1. Small-scales contribute to secular variation

Much of what we know about flow and magnetic field within the core is deduced from the analysis of the secular variation of the magnetic field observed at the surface of the Earth (see Chapter by Holme (2015)). The magnetic field at the core-mantle boundary is determined only up to degree 13 of the spherical harmonics (corresponding to a wavelength of about $2\pi\times3500/13 =$ 1700km at the top of the core). Its time derivative is known up to degree 10 for the most recent epoch. One aims at reconstructing the large-scale velocity U by inverting the frozen flux induction equation of the radial component of the magnetic field B_r at the core-mantle boundary:

$$\partial_t B_r + \boldsymbol{\nabla}_H \cdot (\boldsymbol{u} B_r) = 0. \qquad (1)$$

The problem is that unresolved small-scale motions can interact with unresolved small-scale magnetic field to contribute to the large-scale induction term of this equation. Eymin and Hulot (2005) show that realistic amplitudes of these two unresolved fields produce representation errors that largely exceed the observational errors. Better models are obtained when these representation errors are taken into account in core flow inversions (Pais and Jault, 2008). It is therefore of interest to get some constraints on the evolution of the velocity and magnetic field with harmonic degree beyond what can be inferred from the observations.

3.2. Small-scales and dynamo action

Mean-field dynamo theories developed in the sixties (Moffatt, 1961; Steenbeck et al., 1966) have demonstrated that the interaction of the small-scales of a turbulent flow in a conducting fluid with the small-scales of the magnetic field they induce can produce a large-scale magnetic field (see Moffatt (1978) for a review). This mechanism is nicely illustrated by the success of the two-scale dynamo experiment in Karlsruhe (Stieglitz and Müller, 2001). Liquid sodium was forced to flow up and down in helicoidal motions in an array of pipes set up to mimic the two-dimensional periodic paving of the G.O. Roberts dynamo (Roberts, 1972). Induction was clearly taking place at the scale of each of the 52 individual 0.21m-diameter pipes. Nevertheless, a large-scale magnetic field was produced at the scale of the complete 1.7m-diameter assembly.

The simplest forms of mean-field dynamo theory predict that isotropic homogeneous turbulent motions in a conducting fluid produce a large-scale electromotive force $\mathcal{E} = \boldsymbol{\alpha} : \langle \boldsymbol{B} \rangle + \boldsymbol{\beta} : \boldsymbol{\nabla} \times \langle \boldsymbol{B} \rangle$, where $\langle \boldsymbol{B} \rangle$ is the large-scale magnetic field, $\boldsymbol{\alpha}$ and $\boldsymbol{\beta}$ are two tensors, which depend upon the turbulent characteristics of the flow, and : is the tensorial dot product. In this view, the α-effect is crucial for enabling the large-scale magnetic field to grow, while the β-effect can increase or decrease the magnetic diffusivity. Parameterized numerical dynamo models relying on these ideas have had a crucial role in explaining the solar cycle, and they are still very useful (see Charbonneau (2005) for a review). However, the lack of scale separation and the expected deviations from isotropy and homogeneity can strongly impact the relevance of this theory for the geodynamo.

3.3. Dissipation and efficiency

In the so-called inertial range of classical turbulence, energy is transferred from the large scales to the small scales, with almost no energy loss. The dissipation of

energy occurs at the smallest scales, where velocity gradients become large enough for viscous forces to balance non-linear inertial terms. The smaller this scale, the higher the dissipation. We examine several alternative scenarios for turbulence in section 8 and show that they yield extremely diverse dissipation rates. The efficiency of convective motions for producing a dynamo therefore strongly depends on the organization of the turbulent velocity and magnetic fields.

3.4. Mixing

Turbulence affects the mixing of fluid parcels and of what they transport. It has therefore received considerable attention in atmospheric and oceanic sciences, where the transport of pollutants or nutrients have an important socio-economical impact. This question has not yet been tackled in studies of core dynamics. However, seismology reveals that layers at the bottom and at the top of the liquid core may have a slightly different composition. How much mixing takes place between these layers and the rest of the core has important geodynamical implications (Alboussière et al., 2010). The observation of the atmospheres of Jupiter and Saturn reveals that zonal bands with alternating wind directions are able to maintain a strikingly different chemical signature, yielding contrasting colors, despite a very active turbulence. We should keep this in mind when considering the fluid inside the cylinder tangent to the inner core.

4. Fundamentals of turbulence

Identified by Feynman as 'the most important unsolved problem of classical physics', turbulence has been the subject of numerous studies over a large part of the XXth century. Unsolved fundamental issues remain, but an impressive corpus of results and models has been acquired (see Frisch (1995) for a review and more). We give here a simple overview of some fundamental aspects of hydrodynamic turbulence (*i.e.*, in the absence of global rotation and magnetic field).

4.1. Energy density spectra and energy cascade

While all turbulent fields undergo large fluctuations in time and space, it has been found that energy density spectra of the flows are robust and universal in hydrodynamic turbulence. In addition, these spectra nicely summarize the scaling properties of the flow and the energy transfer that takes place. Defining k as the (scalar) wavenumber of the flow in the Fourier space, the energy density $E(k)$ is defined by:

$$\tilde{E} = \frac{1}{2}\langle u^2 \rangle = \int_0^\infty E(k)\, dk, \tag{2}$$

where $\tilde{E}$ is the energy of the fluctuations per unit mass. The theory of 'universal turbulence' was established by Kolmogorov (1941b). The basic idea is that there should be a wavenumber k_0 above which turbulence does not depend upon how energy is fed to the flow. The only thing that counts is the mean power per unit mass ϵ it provides, and which is also dissipated in the stationary regime. In this idealized view, universal turbulence should thus be isotropic and homogeneous, and it should have a self-similar character.

The smaller length scale at which dissipation operates is called the Kolmogorov scale, with wavenumber k_D. It depends upon ϵ and the kinematic viscosity ν. Viscous dissipation per unit mass can be written as $\nu(\boldsymbol{\nabla u})^2$, which we express as $\nu k_D^2 \left(u(k_D)\right)^2$ at the k_D wavenumber. The typical velocity $u(k_D)$ is obtained by stating that the Reynolds number at this scale should be about 1 for dissipation to occur, yielding $u(k_D) \sim \nu k_D$. We thus obtain:

$$k_D = \left(\frac{\epsilon}{\nu^3}\right)^{1/4}. \tag{3}$$

The main assumption of Kolmogorov is then that, in the wavenumber range between the injection scale and the dissipation scale ($k_0 \ll k \ll k_D$), all statistically averaged quantities at wavenumber k are a function of k and ϵ only. Dimensional analysis then commands:

$$E(k) = C_K \epsilon^{2/3} k^{-5/3}, \tag{4}$$

which is the famous $k^{-5/3}$ law derived by Obukhov (1941), and where C_K is a dimensionless constant called the 'Kolmogorov constant'. It has been found that a wide class of actual turbulent flows follow this law, sometimes over many decades in wavenumber, and C_K has been measured to lie between 1.5 and 2.

The k-power-law dependence of $E(k)$ is a signature of self-similarity in this wavenumber range, called the inertial range, along which energy cascades from the injection length scale down to the dissipation scale. Self-similarity extends to higher order 'structure functions' $S_p(\ell)$, which are defined as $S_p(\ell) = \langle \delta u^p(\ell) \rangle$, where $\langle\rangle$ denotes a statistical average, and $\delta u(\ell)$ is the velocity difference measured between two points separated by a distance ℓ. Longitudinal velocity differences are usually considered (*i.e.*, difference in the projection of velocity on the line that links the two points). Measurements yield:

$$S_p(\ell) \sim \ell^{\zeta_p}, \tag{5}$$

where the exponents ζ_p appear to be universal. $E(k)$ is directly related to $S_2(\ell)$, so that $\zeta_2 = 2/3$ for Kolmogorov $E(k)$ spectra. In fact, under Kolmogorov's hypotheses, one gets $\zeta_p = p/3$ for all p. Measurements indicate that the actual ζ_p exponents clearly deviate from this prediction as p increases (Anselmet et al., 1984). The high-order structure functions are related to the tails of the probability distribution function (*PDF*) of velocity differences. For small separation distances ℓ these distributions strongly deviate from normal distributions, showing a larger influence of intermittent 'rare' events.

4.2. Structures

The apparition of flow structures is an unavoidable consequence of the break of symmetry that characterizes the instabilities at the origin of turbulence. Anyone who has looked at turbulent flows in a river or in the air will retrieve the image - nicely illustrated by Leonardo da Vinci - that vortices or eddies are the building bricks of hydrodynamic turbulence. Eddies come in a large range of sizes. They are usually longer than wide, and can even stretch into vorticity filaments. The core of an eddy has a strong but relatively homogeneous vorticity $\boldsymbol{\omega} = \boldsymbol{\nabla} \times \boldsymbol{u}$, while the opposite holds on its edges. There, the shear between eddies nucleates smaller eddies. Long filaments can also break into shorter filaments. In this way, energy cascades down to small scales, where dissipation occurs.

With this in mind, it does not seem obvious that, even if vortices can take all sizes and orientations, the embedding of essentially one-dimensional structures (vorticity filaments) into three-dimensional space, will have no influence on the statistically averaged quantities at wavenumber k, as originally assumed by Kolmogorov. This idea is the starting point of She and Leveque (1994). They show that vorticity filaments dissipate the available surrounding energy very efficiently by forcing the lower intensity eddies into an essentially bidimensional flow around them. Vorticity filaments are relatively rare, as they correspond to eddies that have had the opportunity to stretch and get stronger. To illustrate this phenomenon, Kaneda and Morishita (2013) report that 33% of the energy dissipation occurs in 5% of the volume in one of the highest Reynolds number Direct Numerical Simulation performed to date. One consequence is that the average moments of the energy dissipation $\langle \epsilon^p(\ell) \rangle$ within a sphere of radius ℓ depends upon the scale ℓ. Self-similarity implies:

$$\langle \epsilon^p(\ell) \rangle \sim \ell^{\tau_p}, \tag{6}$$

where the exponents τ_p should again be universal. Kolmogorov's hypothesis that all statistically averaged quantities only depend upon scale and mean dissipation ϵ, implies $\langle \epsilon^p(\ell) \rangle = \epsilon^p$, independent of ℓ (*i.e.*, $\tau_p = 0, \forall p$). If this hypothesis is relaxed to take into account intermittency, the 'refined similarity hypothesis' derived by Kolmogorov (1962) yields a relation between the ζ_p and τ_p exponents:

$$\zeta_p = p/3 + \tau_{p/3}. \tag{7}$$

She and Leveque (1994) derived expressions for τ_p and hence for ζ_p that are in excellent agreement with the measurements:

$$\zeta_p = p/9 + 2\left[1 - \left(\frac{2}{3}\right)^{p/3}\right]. \tag{8}$$

Note that the $-5/3$ exponent of k in the expression for $E(k)$ is hardly modified by this extension, and that the ζ_3 exponent is always 1, as it can be derived with no adjustable parameter from the Navier-Stokes equation in some conditions (see Kolmogorov (1941a); Frisch (1995); Kaneda and Morishita (2013)), yielding Kolmogorov's equation (also called the four fifth law):

$$S_3(\ell) = -\frac{4}{5}\epsilon\ell. \tag{9}$$

Turbulence can be strongly modified by the presence of global rotation or/and magnetic field. Although we are still lacking a thorough description of turbulence under such conditions, we will unravel and discuss some of its known or inferred properties in section 8, and try to get closer to a description that applies to the Earth's core.

5. Tools for turbulence

5.1. Direct Numerical Simulations

Direct Numerical Simulations (DNS) consists in fully solving the equations of the problem, namely the Navier-Stokes equation together with the induction and the codensity equations (see §7.1). Best Navier-Stokes simulations reach an impressive resolution of 4096^3 (Kaneda and Morishita, 2013). The size of the resulting discrete problem for the Earth's core is such that we cannot hope a DNS at the real parameters anytime soon: from the core size to the Ekman layer thickness, 6 orders of magnitude in length and time scales must be resolved.

The problem is made even worse by the need to take into account the spherical geometry and the coupling with the induction equation. Nevertheless, DNS of the geodynamo have proven very useful, as exposed

in the Chapter by Christensen and Wicht (2015). They clearly demonstrate the role of rotation in the generation of a large-scale magnetic field, dominated by a dipole aligned with the axis of rotation. Furthermore, scaling relationships derived from these simulations seem to indicate that their output is independent of the precise values of the diffusion coefficients (Christensen and Aubert, 2006), giving hope that relevant asymptotic regimes are attained even though diffusivities are far larger than the values expected for the core.

Some DNS have tackled the question of small-scale turbulence in core situations. Following the theoretical work of Braginsky and Meytlis (1990), StPierre (1996) performed DNS of turbulence in the presence of both rotation and magnetic field. He found that buoyant patches rapidly break up into plate-like structures elongated in the directions of the rotation axis and of the prevailing magnetic field. Giesecke (2007) found similar results. However, it is not clear how a turbulent cascade of energy can build upon such structures. Besides, these simulations do not take into account the fact that rotation and magnetic field characteristic times are several orders of magnitude apart in the core (see section 8).

MHD turbulence is very difficult to model. The magnetic field imposes a strong anisotropy, which can be used to reduce the full MHD equations. Energy spectra for 'weak' and 'strong' MHD turbulence have been obtained this way (see Tobias et al. (2013) for a review).

Even though DNS are not able to simulate the core, they can offer some insight in the dynamics, and in particular they give hints to support the scenarios that we elaborate based on various studies in different dynamical regimes. Figures 1 and 2 display a snapshot of a full geodynamo DNS computed for fairly extreme parameters that get closer to core values. It shows thinner elongated coherent structures in the velocity field than in simulations at milder Ekman numbers. It strongly supports the large-scale, high magnetic Reynolds number (Rm, see table 2) picture, where the Coriolis force dominates.

5.2. Laboratory experiments

The exploration of highly turbulent flows is possible in laboratory experiments. Very long time series are easily obtained. The main problem is often to access the quantities that best document turbulent behaviour. Laboratory experiments have played and are still playing an important role in the exploration of the dynamics of geophysical and astrophysical fluids. A review of the experimental results that shed light on core dynamics is given in Chapter by Cardin and Olson (2015).

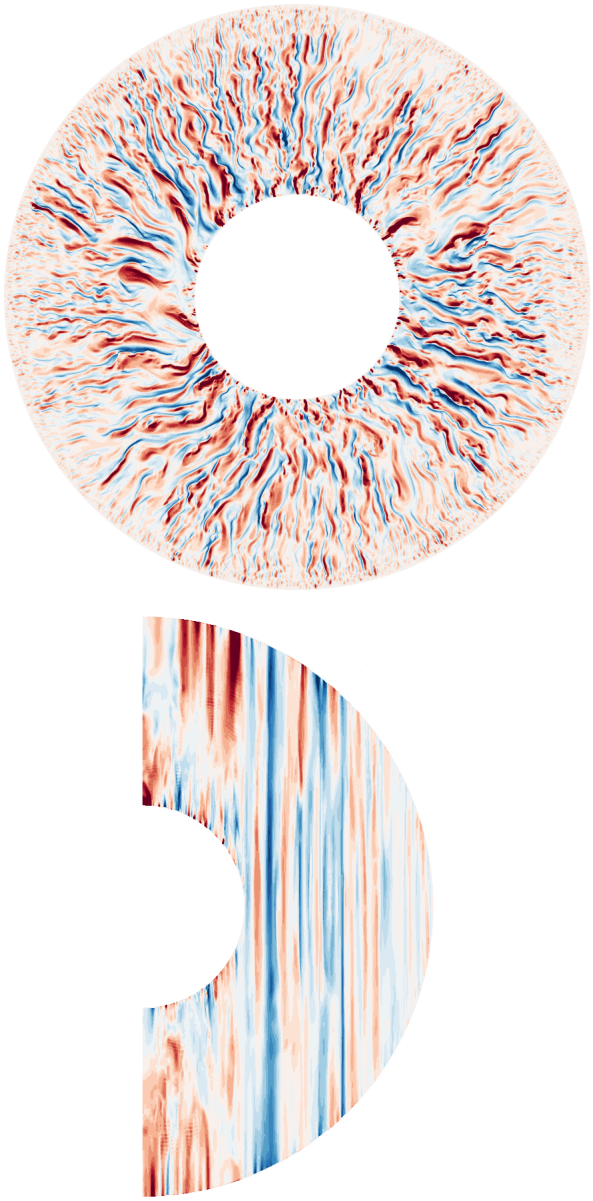

Figure 1: Cylindrical radial velocity component u_s in the equatorial plane (top) and a meridional plane (bottom). Snapshots from a dynamo DNS at $E = 10^{-7}$, $Pm = 0.1$, $Pr = 1$, $Ra = 2.4 \times 10^{13}$ (see table 2 for definition of these numbers using ℓ the radial distance between inner shell and outer shell), using spherical harmonic expansion up to degree 893 and 1024 radial shells.

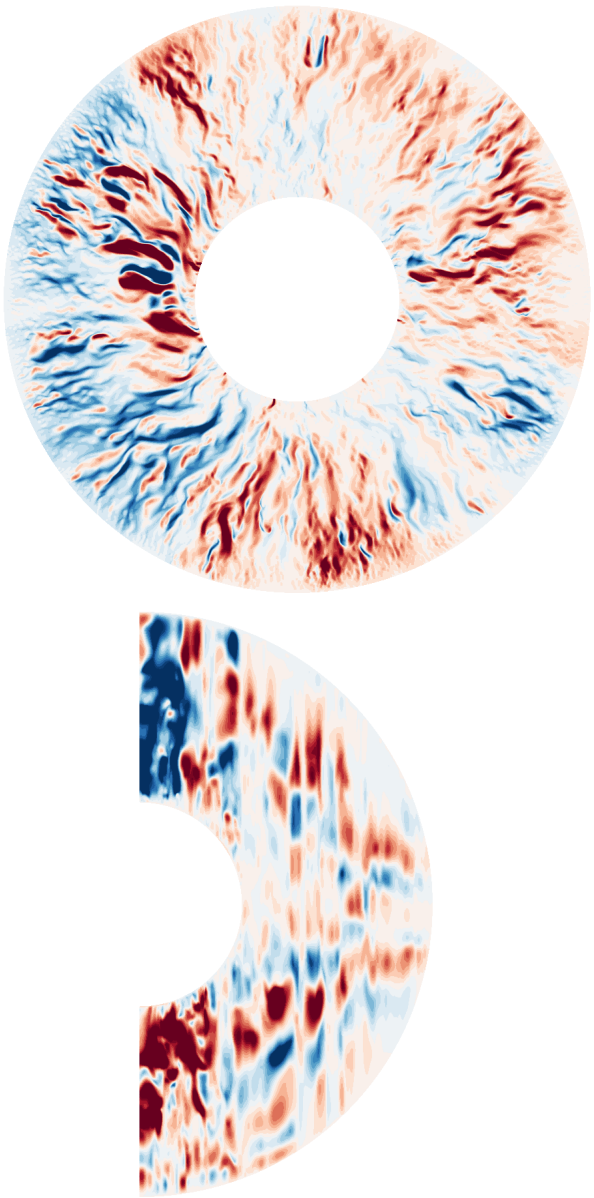

Figure 2: Cylindrical radial magnetic field component B_s in the equatorial plane (top) and a meridional plane (bottom). Snapshots from a dynamo DNS at $E = 10^{-7}$, $Pm = 0.1$, $Pr = 1$, $Ra = 2.4 \times 10^{13}$ (see table 2 for definition of these numbers using ℓ the radial distance between inner shell and outer shell), using spherical harmonic expansion up to degree 893 and 1024 radial shells.

Early experiments used local intrusive probes and provided key measurements on several features of turbulence. For example, Anselmet et al. (1984) determined the structure exponents ζ_p in a turbulent jet up to $p = 10$, providing a strong motivation for theoretical improvements (Frisch, 1995). The first experimental wavenumber energy density spectra for MHD turbulence in an applied magnetic field were measured by Alemany et al. (1979) using velocity probes attached to a grid moving in a column of mercury placed within a solenoid. They found a kinetic energy spectrum $E_u(k) \sim k^{-3}$ demonstrating the strong damping of fluctuations by the applied magnetic field in the low magnetic Reynolds number regime.

Recent experiments rely on optical methods based on Particle Image Velocimetry (*PIV*), which have evolved into very efficient tools (see Westerweel et al. (2013) for a recent review) and brought new constraints on turbulence in transparent fluids, such as air and water. Let us cite, as an example, the determination of the structure coefficients of Lagrangian velocity increments in a von Kármán flow (Xu et al., 2006), and the structure coefficients of velocity increments in shallow layer rotating turbulence (Baroud et al., 2003). These methods have also been very useful for establishing the idea that the mixing of potential vorticity plays a major role in shaping zonal flows in rotating fluids (Aubert et al., 2002). Recently, using a transparent electrolyte and a superconducting magnet, Andreev et al. (2013) demonstrated that PIV methods can be used in MHD experiments.

Advances in handling Helium gas at low temperatures has opened a new way for exploring thermal convection at very high Rayleigh numbers. As we will see in section 8.2, the Rayleigh number measures the vigor of convection. Niemela et al. (2000) report heat transfer measurements for an incredible range of 11 decades in Rayleigh number from 10^6 to 10^{17}, displaying a very simple power-law dependence of the Nusselt number $Nu = 0.124\, Ra^{0.309}$ over the full range (the Nusselt number measures the convective heat transfer efficiency). They also provide nice evidence for a Kolmogorov $f^{-5/3}$ frequency power spectrum of temperature fluctuations at $Ra = 6 \times 10^{11}$.

For experiments with liquid metals, which are essential for investigating magnetohydrodynamic turbulence, acoustic Doppler velocimetry has proven very useful (Brito et al., 2001; Stefani et al., 2009; Brito et al., 2011). Interestingly, in such experiments, induced magnetic fields resulting from the interaction of the flow with a weak imposed magnetic field, which can be measured outside the experiment, provide an information on the hydrodynamic flow that would be difficult to retrieve

otherwise. For example, Kelley et al. (2007) discovered that specific inertial modes were excited in a rotating spherical Couette flow experiment using liquid sodium as a working fluid. These modes appear to be excited by critical layers attached to the Stewartson layer that accommodates the angular velocity jump between the inner sphere and the outer sphere when both rotate (Rieutord et al., 2012).

When a strong dipolar magnetic field is applied in the same Couette geometry, as in the DTS experiment (see Brito et al. (2011)), modes are also observed (Schmitt et al., 2008, 2013), but the modes are strongly affected by the Lorentz force. The DTS experiment also demonstrates that turbulence is strongly hampered under the action of both global rotation and a strong magnetic field (Nataf et al., 2008; Nataf and Gagnière, 2008).

The pioneer dynamo experiments of Riga (Gailitis et al., 2001) and Karlsruhe (Stieglitz and Müller, 2001) have not only demonstrated the self-sustained dynamo process in the Lab, they also have opened the way to using liquid sodium as a working fluid in MHD and dynamo experiments. Several teams across the world have followed their example, and set up sodium experiments in which the mean flow is accompanied by fluctuations of a similar amplitude (see Verhille et al. (2010); Lathrop and Forest (2011) for recent reviews). Spontaneous generation of a magnetic field has thus been observed in the VKS experiment in Cadarache (Monchaux et al., 2007), but only when the impellers are ferromagnetic. A variety of different dynamical regimes has been observed in this device, including spectacular chaotic reversals of the magnetic field (Berhanu et al., 2007). One of the main lessons from these studies is that turbulent fluctuations appear to hinder the dynamo action that the mean flow should produce if it were alone, Besides, ohmic dissipation remains high in these experiments, and Alfvén waves are too damped to play a dynamic role, except when the device is placed in a very strong magnetic field (Alboussiere et al., 2011). Using plasma as a working fluid opens new possibilities, which are under investigation (Spence et al., 2009).

5.3. Observations

Unfortunately, no observations of the internal geomagnetic field are possible at small scales, mostly because of the crustal field that overprints the small-scale core field. Observations of turbulence in other systems is thus required, to gain insight in what happens in the Earth's core.

Characterization of turbulence in the Earth's atmospheric boundary layer was probably the first target of detailed analyses of turbulence. The first measurements of turbulent fluxes were performed in Australia by the eddy correlation technique (Swinbank (1951), see Hogstrom (1996) for a review). All these observations shed light on the universal behavior of turbulence in natural environments, showing for example that the von Kármán constant $K = u_*/(z\,\partial_z u_H)$, relating the amplitude of turbulent fluctuations u_* to the vertical gradient of mean horizontal velocity $\partial_z u_H$ in the inertial sublayer, is constant and equal to its laboratory value of 0.4, irrespective of the roughness of the ground, as expected from the scale-invariant properties of universal turbulence (Lo et al., 2005).

Later on, compilations of data from commercial aircraft flights demonstrated that winds and temperature follow Kolmogorov's $k^{-5/3}$ law for wavelengths from a few kilometers up to 400km, steepening to a k^{-3} law at larger scales (Nastrom and Gage, 1985). Coupling these observations with simulations from General Circulation Models opens the way to determining the actual energy fluxes responsible for this behaviour (Augier and Lindborg, 2013).

Space exploration of the solar system has revealed the fantastic dynamics of the atmospheres of Jupiter and Saturn, and opened the way for detailed analyses of their turbulent behavior. The long-term stability of the strong and numerous zonal jets they display remains a strong driver for modeling turbulence on a rotating sphere (see Vasavada and Showman (2005) for a review).

Combining observations and high-performance numerical modeling, the re-analysis of ocean circulation nicely illustrates the role of quasi-geostrophic mesoscale eddies in the dynamics of the ocean. In particular, zonal motions resulting from the interaction of turbulent eddies have recently been detected (Maximenko et al., 2005).

The solar wind is a great laboratory for MHD turbulence, as reviewed by Bruno and Carbone (2005). Even though it is a collisionless plasma, MHD turbulence is expected for frequencies below 0.1 Hz. Two types of solar winds must be distinguished. The fast wind originates from polar regions of the Sun and has mean velocities about twice as fast as the slow wind coming from equatorial regions. The temporal fluctuations in the solar wind have been measured by several probes starting in the sixties. The measurements show three regimes in the temporal energy spectrum $E(f) \sim f^{\alpha}$: the lowest frequencies have $\alpha \simeq -1$ for period about a day or longer, while higher frequencies follow $\alpha \simeq -3/2$ for the fast wind and $\alpha \simeq -5/3$ for the slow wind. Finally at periods around a few seconds $\alpha \simeq -2$ is found. The transition between the first two regimes is rather sharp

and is located around 10 − 16 hours, depending on the distance from the Sun. The fluctuations are found to be anisotropic, with much weaker fluctuations along the local magnetic field. A strong correlation exists between the velocity and the magnetic fluctuations, especially for the fast wind, showing the predominance of (incompressible) Alfvén waves in solar wind turbulence. At large distance from the Sun, magnetic field fluctuations are twice more energetic than velocity fluctuations. This observation remains puzzling, although it is also observed in some dynamo simulations.

5.4. Shell models

Shell models of turbulence originated in the seventies, as a tool to assess the statistical properties of universal turbulence. In these models structures are ignored, as all fields are projected on a suite of shells of wavenumber k_n in the spectral domain. The sequence of wave numbers k_n is chosen to be geometric, thus enabling a wide range of length-scales to be covered with a limited number of grid points. One takes into account the symmetries and conservation laws that pertain to the type of turbulence under study (2D or 3D hydrodynamic turbulence, magnetohydrodynamic turbulence, etc). The game is then to choose the rules that govern the transfer between shells, which mimic the nonlinear interactions between the various fields of the various shells. The phenomenon of intermittency described above can be recovered in shell models.

Shell models have received a lot of attention in the past decade, and extensions to MHD and rotating turbulence have been worked out (see Plunian et al. (2013) for a thorough review). Shell models are particularly appealing for exploring MHD turbulence in fluids with a very small (or very large) magnetic Prandtl number, for which Direct Numerical Simulations are hopeless because of the large range of scales to be resolved. The magnetic Prandtl number $Pm = \nu/\eta$ is the ratio of kinematic viscosity over magnetic diffusivity. It is of order 10^{-5} for liquid iron in the core. As an example, Plunian and Stepanov (2010) explored how the ratio of magnetic to viscous dissipation varies with the magnetic Prandtl number. They found that, under model assumptions, magnetic dissipation is at least ten times larger than viscous dissipation for core values.

5.5. Plume model

In contrast with the approach we just described, David Loper and others focused on buoyant plumes envisioned as the elementary structure at the origin of turbulent motions in the core. The analysis of the dynamics of such plumes in core conditions led David Loper to infer that rising plumes would have dimensions in the range 10 − 1000m, typical relative density anomalies between 10^{-10} and 10^{-8}, and upwelling velocities from 10^{-3} to 10^{-1}m/s, depending on actual core properties. At the base of the convecting outer core, plumes would occupy a fraction of the surface between 10^{-5} and 10^{-1}. The reader is referred to David Loper's Chapter (Loper, 2007) in the first edition of the Treatise on Geophysics for a complete description of the plume model.

6. Parametrization of turbulence

Numerical simulations are limited by the available memory of the computer and its computing power. The more turbulent the flow, the larger the scale range. Therefore, direct numerical simulations that resolve all the spatial scales down to the viscous dissipation scale (the limit of turbulent small scales) cannot reach strongly turbulent regimes. If one could capture the (statistical) effect of turbulent small scales on the larger scales, and properly predict the turbulent small scale state corresponding to the large scales that produce it, we could in principle parametrize the effect of small scale turbulence.

If several parameterizations for purely hydrodynamic, homogeneous, isotropic turbulence are available and used in hydrodynamic simulations, or in the MHD regime at low Rm and low interaction parameter (e.g. Ponty et al., 2005), we should at least question their use for modeling the Earth's core.

On one hand, if we target the dynamics to the small scales inside the Earth's core, we will see that the turbulence inside the Earth's core may never reach the parameter-space region where simple hydrodynamic turbulence takes place (see §8). Thus we are left with a challenging task: finding a necessarily anisotropic parametrization that depends on the local magnetic field as well as on the global rotation.

On the other hand, the current numerical geodynamo models do not seem to operate in such a regime, and hydrodynamic turbulence may indeed be important for the small scales in these models. Indeed, even with a magnetic field and a large magnetic diffusivity, part of the flow which is aligned with the magnetic field will not produce electric current and dissipation. Viscosity is the only isotropic dissipation in such systems. Furthermore, the smaller the scale, the smaller the influence of the magnetic field (interaction parameter), hence the smallest scales may only rely on hydrodynamic turbulence for the energy to reach the viscous dissipation scale.

Here, we wish not to provide a detailed theoretical framework for sub-grid scale modeling, but rather list a few approaches that have been used to perform numerical simulation of the Earth's core. With the above limitations in mind, we describe two approaches.

6.1. Hyper-diffusivities or eddy-diffusivities

Hyper-diffusivity is the simplest form of parametrization of small-scale turbulence, where the effect of unresolved small scales are expressed as an enhanced diffusivity on the resolved scales. In hydrodynamical turbulence, where the interactions are mostly local (which means that a given scale is mostly influenced by its neighboring scales), such enhanced diffusivity can arguably be restricted to the smallest resolved scales. Although there is no physical justification for the use of hyper-diffusivity, there is a practical one: with increased viscosity at small scales, a numerical simulation is able to dissipate more energy, which would have been the main effect of smaller unresolved scales.

The first geodynamo simulation by Glatzmaier and Roberts (1995) made use of hyper-diffusivity at all scales, which is arguably both a concern and not really a small-scale parametrization, but it allowed to run a full geodynamo model on the computers of the early nineties. A more reasonable approach is to restrict the use of hyper-diffusivity only at the smaller scales. Following the pioneers, many authors use a hyper-diffusivity of the type $\nu(l) = \nu_0(1 + a(l - l_0)^n)$ for $l > l_0$ and $\nu(l) = \nu_0$ for $l \leq l_0$, where l is the spherical harmonic degree (angular wave number) and a, l_0 and n are adjustable parameters. It must be emphasized that this is still an isotropic viscosity but its value depends only on l and not on the radial spatial size (for practical reasons). This (historical) formula may seem overly complicated, with three adjustable parameters. A simpler, more elegant form for hyper-diffusivity with self-similarity properties would be:

$$\nu(l) = \begin{cases} \nu_0 & \text{for } l \leq l_0 \\ \nu_0\, q^{l-l_0} & \text{for } l > l_0 \end{cases} \tag{10}$$

which has only two independent parameters l_0 and q.

Finally, we want to emphasize that such an approach (anisotropic hyper-diffusivity) must be used with care, as it has been shown to have significant effect on the dynamics (Grote et al., 2000).

6.2. Large Eddy Simulations

Attempts have been made to apply models of hydrodynamic turbulence to model the subgrid-scales of the peculiar turbulence occurring inside the Earth's core. A rather successful model is the Large Eddy Simulations (LES) using a similarity model, where the energy transfer due to the interaction with smaller, unresolved scales are estimated by the transfer that actually occurs between the small but resolved scales of the simulation. This has the huge advantage over the eddy-diffusivity technique that it can capture the anisotropic nature of transfer between scales. Although the idea seems interesting, these LES models are still in an early development stage. Indeed, they are constantly compared to higher resolution DNS, and there are many important tunable parameters (e.g. Buffett, 2003; Chen and Jones, 2008; Matsui and Buffett, 2012). Furthermore, the DNS they compare with are far from the dynamical regime expected in the Earth. The presence of boundaries, where turbulence is no more homogeneous, is also a difficulty for LES models.

Currently LES can be useful to run simulations over a long time period, where the corresponding DNS is feasible but slower. By comparing with a short term DNS and tuning the subgrid-scale model to reproduce it, we can then trust the LES model for the long term simulation.

A greater challenge for these models is to actually predict rather than reproduce, which would be a major breakthrough, but it is not clear whether or not they will ever succeed. A key to success might be to ensure that the smallest resolved scales are actually in the low Rm regime, where the self-similar hypothesis is more likely to hold.

7. Equations, time and length-scales

7.1. Equations

The velocity field $\boldsymbol{u}$ describing the flow of the Earth's liquid core of density ρ is governed by the Navier-Stokes equation including the Coriolis force (due to the rotation rate Ω of the planet), the Lorentz force and the buoyancy force. It is supplemented with the mass-conservation equation, simplified in the anelastic framework (Gilman and Glatzmaier, 1981):

$$\begin{aligned} \partial_t \boldsymbol{u} + (\boldsymbol{u}\cdot\boldsymbol{\nabla})\boldsymbol{u} + 2\boldsymbol{\Omega}\times\boldsymbol{u} = \\ -\boldsymbol{\nabla}\Pi + C\boldsymbol{g} + (\boldsymbol{B}\cdot\boldsymbol{\nabla})\boldsymbol{B}/\rho\mu_0 + \nu\nabla^2\boldsymbol{u} \end{aligned} \tag{11}$$

$$\boldsymbol{\nabla}\cdot(\rho\boldsymbol{u}) = 0 \tag{12}$$

where Π is a reduced pressure including other potential forces (including the centrifugal force and magnetic pressure).

The evolution of the divergence-free magnetic field $\boldsymbol{B}$ in this liquid metal is governed by the induction equation.

$$\partial_t \boldsymbol{B} + (\boldsymbol{u}\cdot\boldsymbol{\nabla})\boldsymbol{B} = (\boldsymbol{B}\cdot\boldsymbol{\nabla})\boldsymbol{u} + \eta\nabla^2\boldsymbol{B} \quad (13)$$

$$\boldsymbol{\nabla}\cdot\boldsymbol{B} = 0 \quad (14)$$

The evolution of the buoyancy is less well-known, as it originates from both chemical and thermal variations, which have different diffusivities. As we are not focusing on the energy injection mechanism details, we can use a single codensity C, with a specified volumic source term S.

$$\partial_t C + (\boldsymbol{u}\cdot\boldsymbol{\nabla})C = \kappa\nabla^2 C - S \quad (15)$$

There are assumptions behind these equations that we would like to make excplicit. For simplicity, the diffusive terms are written as a simple Laplace operator, which implies an homogeneous diffusivity. As the diffusivities are very small, these terms are important only at small scales, while we expect the variations of the diffusivity coefficient to be moderate over the depth of the core. The codensity formulation hides the difference between thermal and chemical diffusivities.

These equations must be completed by boundary conditions. Boundary conditions are important and can control the dynamical state of the system (see e.g. Sakuraba and Roberts, 2009), but they are thought to have only an indirect effect on the small scale turbulence.

7.2. Ordering of forces in the Earth's core

For the Earth's core, the order of magnitude of the different terms can be evaluated. We will focus on the scale-dependence of this ordering, that may help to understand the dynamics of the small scales. From the inversion of the geomagnetic secular variations (see Chapter by Holme (2015)), we have an estimate of the large-scale velocity field at the core surface: $U \sim 15\,\mathrm{km/yr} \sim 5\times10^{-4}\,\mathrm{m/s}$. More recently, the observation of torsional oscillations by Gillet et al. (2010) has given us an estimate of the magnetic field strength deep inside the core ($B_0 \sim 3\times10^{-3}\,\mathrm{T}$). The buoyancy force drives the system, but it is hard to assess its strength and compare it to other forces. Indeed, convection tends to smooth the codensity through mixing. We will rather focus on the velocity and magnetic fields as a result from this buoyancy, and try to understand how they organize at various scales.

For doing so, we build ℓ-scale dimensionless numbers, which compare the weight of the various terms of the equations at a typical length-scale ℓ. This length-scale can be related to the wave-number k in a Fourier decomposition by $\ell = 2\pi/k$. We find it convenient to express these numbers as ratios of characteristic times, which are functions of ℓ. For example, diffusive phenomena will have time-scale τ and length-scale ℓ related by:

$$\tau_\nu(\ell) = \ell^2/\nu, \quad (16)$$

where we have picked here the diffusion of momentum, governed by the kinematic viscosity ν. We can thus define an ℓ-scale **Reynolds number**

$$\mathrm{Re}(\ell) = \frac{u(\ell)\ell}{\nu} = \frac{\tau_\nu(\ell)}{\tau_u(\ell)},$$

which compares advection to diffusion of momentum at the ℓ-scale. Other relevant times are listed in Table 1 and will be introduced in the coming sections, while ℓ-scale dimensionless numbers are listed in Table 2.

7.2.1. Coriolis force

The ℓ-scale **Ekman number**

$$E(\ell) = \frac{\nu}{\ell^2\,\Omega} = \frac{t_\Omega}{\tau_\nu(\ell)}$$

compares viscous forces to the Coriolis force. It is the ratio of the rotation time t_Ω over the viscous diffusion time $\tau_\nu(\ell)$. This number is tiny at large scales and reaches unity for scales comparable to the laminar Ekman layer thickness, estimated to be less than a meter in the Earth's core. It is unlikely that turbulence reaches such small scales, because dissipation would be too large (see section 8). This means that the Coriolis force is important at every scale, including the dissipative scales.

The ℓ-scale **Rossby number**

$$Ro(\ell) = \frac{u(\ell)}{\ell\,\Omega} = \frac{t_\Omega}{\tau_u(\ell)}$$

compares eddy entrainment force to the Coriolis force. It is also the ratio of the rotation time over the eddy turnover time at length-scale ℓ. For the scale of the whole core, we have $Ro_0 \sim 10^{-6}$, a small value showing the predominance of the Coriolis force at large scales, which will eventually decrease toward smaller scales (if we assume that $u(\ell)/\ell$ increases as ℓ decreases). Depending upon the evolution of the typical velocity $u(\ell)$ with scale ℓ, it may or may not reach values of order one or more, which would mark a transition from rotation dominated turbulence to 3D turbulence.

notation	expression	description
$\tau_\nu(\ell)$	ℓ^2/ν	viscous time
$\tau_\eta(\ell)$	ℓ^2/η	magnetic diffusion time
$\tau_\kappa(\ell)$	ℓ^2/κ	thermal diffusion time
$\tau_D(\ell)$	ℓ^2/D	compositional diffusion time
$\tau_\rho(\ell)$	$\sqrt{\frac{\ell}{g}\frac{\rho}{\lvert\Delta\rho\rvert}}$	buoyancy time
t_Ω	$1/\Omega$	rotation time (independent of ℓ)
$\tau_{Rossby}(\ell)$	$r_o/\Omega\ell$	Rossby wave propagation time / bidimensionalization time
$\tau_{Alfven}(\ell)$	$\ell\sqrt{\rho\mu_0}/B_0$	Alfvén wave propagation time (large-scale magnetic field)
$\tau_u(\ell)$	$\ell/u(\ell)$	eddy turnover time, regime-dependent
$\tau_b(\ell)$	$\ell\sqrt{\rho\mu_0}/b(\ell)$	Alfvén wave collision time, regime-dependent

Table 1: Characteristic times at length scale ℓ. Symbols and properties as defined in the Overview Chapter (Olson, 2015): ρ, ν, κ, D and η (noted λ in the Overview) are respectively the density, kinematic viscosity, thermal diffusivity, compositional diffusivity and magnetic diffusivity of liquid iron at core conditions. r_o is the radius of the outer core, g is gravity, Ω the angular velocity of the Earth, and B_0 the intensity of the large-scale magnetic field inside the core. $u(\ell)$ and $b(\ell)$ are the eddy turnover time and magnetic field intensity at length-scale ℓ, respectively, which we try to determine for various turbulence scenarios.

notation	expression	time ratio	description
$\mathrm{Re}(\ell)$	$\frac{u(\ell)\ell}{\nu}$	$\frac{\tau_\nu(\ell)}{\tau_u(\ell)}$	Reynolds number
$E(\ell)$	$\frac{\nu}{\ell^2\Omega}$	$\frac{t_\Omega}{\tau_\nu(\ell)}$	Ekman number
$Ro(\ell)$	$\frac{u(\ell)}{\Omega\ell}$	$\frac{t_\Omega}{\tau_u(\ell)}$	Rossby number
$\mathrm{Rm}(\ell)$	$\frac{u(\ell)\ell}{\eta}$	$\frac{\tau_\eta(\ell)}{\tau_u(\ell)}$	magnetic Reynolds number
$n(\ell)$	$\frac{b^2(\ell)}{\rho\mu_0 u^2(\ell)}$	$\frac{\tau_u^2(\ell)}{\tau_b^2(\ell)}$	interaction parameter (small-scale magnetic field)
$N(\ell)$	$\frac{B_0 b(\ell)}{\rho\mu_0 u^2(\ell)}$	$\frac{\tau_u^2(\ell)}{\tau_{Alfven}(\ell)\,\tau_b(\ell)}$	Interaction parameter (large-scale magnetic field)
$\Lambda(\ell)$	$\frac{b(\ell)B_0}{\rho\mu_0 u(\ell)\Omega\ell}$	$\frac{\tau_u(\ell)\,t_\Omega}{\tau_b(\ell)\,\tau_{Alfven}(\ell)}$	Elsasser number
$Lu(\ell)$	$\frac{\ell B_0}{\eta\sqrt{\rho\mu_0}}$	$\frac{\tau_\eta(\ell)}{\tau_{Alfven}(\ell)}$	Lundquist number
$\lambda(\ell)$	$\frac{B_0}{\sqrt{\rho\mu_0}\Omega\ell}$	$\frac{t_\Omega}{\tau_{Alfven}(\ell)}$	Lehnert (or magnetic Rossby) number
$Ra(\ell)$	$\frac{(-\Delta\rho/\rho)g\ell^3}{\kappa\nu}$	$\frac{\tau_\kappa(\ell)\,\tau_\nu(\ell)}{\tau_\rho^2(\ell)}$	Rayleigh number
Pr	ν/κ		Prandtl number (independent of ℓ)
Pm	ν/η		magnetic Prandtl number (independent of ℓ)

Table 2: ℓ-scale dimensionless numbers. One recovers the classical expression of these numbers at the integral scale r_o by setting $\ell = r_o$. These numbers are also expressed as ratios of characteristic ℓ-scale times, which are defined in Table 1.

7.2.2. Magnetic induction

The ℓ-scale **magnetic Reynolds number**

$$\mathrm{Rm}(\ell) = \frac{u(\ell)\,\ell}{\eta} = \frac{\tau_\eta(\ell)}{\tau_u(\ell)}$$

compares magnetic induction to magnetic diffusion in the induction equation. Evaluated at the largest scale, we have $\mathrm{Rm}_0 \sim 10^3$ meaning that a dynamo could take place in the Earth's core. At such scales the magnetic field has a dynamics of its own and is not a slave of the velocity field. $\mathrm{Rm}(\ell)$ decreases with decreasing scale and when it drops below unity, the magnetic field evolution will be mostly dissipative.

The ℓ-scale **interaction parameter**

$$n(\ell) = \frac{b^2(\ell)}{\rho\mu_0\,u^2(\ell)} = \frac{\tau_u^2(\ell)}{\tau_b^2(\ell)}$$

is the ratio of the Lorentz force to the inertial force. When there is a dominant large-scale magnetic field B_0, one can define another interaction parameter:

$$N(\ell) = \frac{B_0\,b(\ell)}{\rho\mu_0\,u^2(\ell)} = \frac{\tau_u^2(\ell)}{\tau_{Alfven}(\ell)\,\tau_b(\ell)}$$

At the largest scale, the ratio of magnetic energy to kinetic energy $N_0 = n_0 \sim 10^4$, which means that the inertial forces are negligible compared to the Lorentz force at large scales.

In small Rm MHD turbulence, the magnetic field is a slave of the velocity field, and the Lorentz force is a linear term. When the magnetic Reynolds number is large, the magnetic field is not just a slave of the velocity field and has its own dynamics. Then the Lorentz force is truly a non-linear term of the system, and the non-linear transfer of energy between scales can happen through the Lorentz force. When both the interaction parameter $N(\ell)$ and $\mathrm{Rm}(\ell)$ are large, we argue that the non-linear transfer of energy between scales is dominated by the Lorentz force, while the inertial force plays a negligible role.

At length-scales ℓ where $\mathrm{Rm}(\ell)$ is small, the induction equation provides an estimate of $b(\ell) \sim u(\ell)B_0\ell/\eta$, where B_0 is the large scale magnetic field. One can thus build a small-scale interaction parameter $N(\ell \to 0) \sim \ell B_0^2/\eta\rho\mu_0 u(\ell)$. If $\mathrm{Rm}(\ell) < 1$, we also have $u(\ell) < \eta/\ell$, so that $N(\ell \to 0) > \ell^2 B_0^2/\eta^2\rho\mu_0 \sim \tau_\eta^2(\ell)/\tau_{Alfven}^2(\ell)$. Applying these relations to the Earth's core, we find that $N > 1$ for $\ell > 30\,\mathrm{m}$. The transition from non-linear energy transfer dominated by the Lorentz force to an energy transfer dominated by advection may occur at a larger scale than this conservative estimate, but we can safely advocate that most of the non-linearity of the core dynamics is due to the Lorentz force.

7.2.3. Lorentz vs Coriolis

We can also compare the Coriolis and Lorentz forces, forming the **Elsasser number**

$$\Lambda(\ell) = \frac{b(\ell)\,B_0}{\rho\mu_0\,u(\ell)\,\Omega\,\ell} = \frac{\tau_u(\ell)\,t_\Omega}{\tau_b(\ell)\,\tau_{Alfven}(\ell)}.$$

The large scale estimate of this ratio gives $\Lambda_0 \sim 0.01$. At scales sufficiently small where $\mathrm{Rm}(\ell) < 1$, the low Rm estimate of $b(\ell)$ gives an Elsasser number independent of the length scale: $\Lambda(\ell \to 0) = B_0^2/\rho\mu_0\eta\Omega \sim 10$. This means that the Coriolis force clearly dominates at large scales but progressively yields to the Lorentz force at small scales.

Using the small Rm expression of $\Lambda(\ell)$ in a dynamo regime is inappropriate and results in wrong estimates of the importance of Lorentz and Coriolis forces (Soderlund et al., 2012).

7.3. Waves and transients

A thorough description of waves that can propagate in the Earth's core is given in the Chapter by Jault and Finlay (2015). If we leave aside sound waves (or seismic waves), there are several other waves that can propagate in our system. First of all, the strong influence of global rotation Ω allows **inertial waves** to exist. They are anisotropic and dispersive, their group velocity $V_\Omega \sim \Omega\ell$ depends on the length-scale ℓ measured in a plane perpendicular to the rotation axis. The propagation of energy by inertial waves occurs mainly along the rotation axis (Davidson et al., 2006), leading to the formation of structures elongated along the rotation axis. The Rossby number, which we have already introduced, also measures the ratio of fluid velocity to inertial wave group velocity.

The presence of the magnetic field allows **Alfvén waves**. Discovered theoretically by Alfvén (1942), these waves couple the velocity field and the magnetic field (see Chapter by Jault and Finlay (2015)). Following the analysis of Tobias et al. (2013), we consider a region at rest with a uniform and constant magnetic field $\boldsymbol{B}_0$. Introducing the Elsasser variables $\boldsymbol{z}^\pm = \boldsymbol{u} \pm \boldsymbol{b}/\sqrt{\rho\mu_0}$, where $\boldsymbol{u}$ and $\boldsymbol{b}$ are the velocity and magnetic fluctuations, the Navier-Stokes and induction equations can be combined to yield:

$$\begin{aligned}(\partial_t \mp \boldsymbol{V}_A \cdot \boldsymbol{\nabla})\,\boldsymbol{z}^\pm + (\boldsymbol{z}^\mp \cdot \boldsymbol{\nabla})\,\boldsymbol{z}^\pm = \\ -\boldsymbol{\nabla}P + \frac{1}{2}(\nu+\eta)\,\nabla^2\boldsymbol{z}^\pm + \frac{1}{2}(\nu-\eta)\,\nabla^2\boldsymbol{z}^\mp.\end{aligned} \tag{17}$$

In the absence of dissipation ($\nu = \eta = 0$), equation 17 describes wave-type motions, which propagate in either directions along the $\boldsymbol{B}_0$ field lines, with the Alfvén wave

velocity $\boldsymbol{V}_A = \boldsymbol{B}_0/\sqrt{\rho\mu_0}$. In a uniform magnetic field, these waves are non-dispersive so that wave-packets of any shape propagate without distortion.

These waves are damped by diffusive phenomena, whose importance is measured by the **Lundquist number**:

$$Lu(\ell) = \frac{B_0 \ell}{\sqrt{\rho\mu_0}(\eta+\nu)} = \frac{\tau_{\eta+\nu}}{\tau_{Alfven}},$$

which compares the diffusive time to the Alfvén propagation time. In liquid metals, where $\eta \gg \nu$, it reduces to $Lu(\ell) = V_A \ell/\eta = \tau_\eta(\ell)/\tau_{Alfven}(\ell)$. When $Lu(\ell) < 1$, Alfvén waves are damped and do not exist anymore. In the Earth's core we have $Lu_0 \sim 10^5$.

The **Alfvén number**

$$A(\ell) = \frac{u(\ell)\sqrt{\rho\mu_0}}{B_0} = \frac{\tau_{Alfven}(\ell)}{\tau_u(\ell)}$$

measures the ratio of fluid velocity to Alfvén wave speed. It is always small in the core ($A(\ell) < 0.01$) meaning that these waves are dynamically important, at least in the directions perpendicular to the rotation axis.

The ratio of Alfvén to inertial wave speed has been called the **Lehnert number** by Jault (2008) and is also called the magnetic Rossby number in Chapter by Roberts (2015):

$$\lambda(\ell) = \frac{B_0}{\sqrt{\rho\mu_0}\,\Omega\,\ell} = \frac{t_\Omega}{\tau_{Alfven}(\ell)}.$$

At large scale, $\lambda_0 \sim 10^{-4}$ means that Taylor columns can form very rapidly (an effect of inertial wave propagation) before the magnetic field can act on the flow (Jault, 2008; Gillet et al., 2011). Once a Taylor column is formed, it can slowly evolve, driven by buoyancy and/or the Lorentz force. At smaller scale, the time to build the Taylor column increases and the columns start to wither. Stationary flow can also escape this Taylor constraint, forming thermal or magnetic winds.

7.4. What should be considered a small scale?

In view of the previous evaluations, there seems to be two main regimes in the core: the high Rm at large scales, and the low Rm at small scales. Based on $\mathrm{Rm}(\ell)$, the transition happens at a length scale $\ell \sim 10\,\mathrm{km}$ or larger, depending on how $u(\ell)$ evolves with ℓ.

In the high Rm regime, the Coriolis force dominates and balances buoyancy, leading to strongly anisotropic dynamics, with predominance of tall coherent structures elongated along the direction of the rotation axis. The kinetic energy is efficiently converted to magnetic energy, and the transfer between scales is ensured by both the Lorentz force and the induction equation.

In the low Rm regime, the Lorentz force dominates the Coriolis force, which still remains important. The dynamical structures are anisotropic, strongly influenced by the direction of the local magnetic field. A significant part of the kinetic energy is dissipated through Joule heating, but motion along the magnetic field remains almost dissipationless. The interaction parameter is still large so the inertial terms are unlikely to be important for the energy transfer between scales, which happens mainly through the Lorentz force. This regime is probably well described by low Rm rotating MHD turbulence at high interaction parameter.

In this picture the buoyancy is merely a shadow that provides the driving force. However, the injection of kinetic energy by buoyancy, which happens presumably at small scales is of particular interest for this problem. In particular it means that the large scale is possibly the result of a non-linear cascade of energy due to the Lorentz force, from small scales to large scale.

The next section will detail the mechanisms and try to paint a broad picture of turbulence in the core from large to small scales.

8. Turbulent regimes for the core

The previous section has shown that the relative importance of the various forces depends upon the length-scale considered. In this section, we try to infer the actual turbulent regimes that should take place in the Earth's core. We consider as given the various diffusivities and the size and rotation rate of the core. We further assume that the large-scale flow velocity is known, from secular variation inversions (see Chapter by Holme (2015)), and that the magnetic field has a dominant large-scale component, whose typical intensity in the core is also known, from the observed velocity of torsional oscillations (Gillet et al., 2010). The actual values we use are listed in Table 3. The questions we address are the following: at what length- and time-scales is the turbulence regime dominated by rotation, by the magnetic field? Can we infer the evolution of flow velocity and small-scale magnetic field in these different regimes? How much energy is dissipated? What is the balance between viscous and ohmic dissipation? Which waves can propagate?

We perform this exercise step by step, introducing the various ingredients that affect turbulence.

8.1. NS-regime diagrams

We introduce a NS-regime diagram or $\tau - \ell$-diagram that helps retrieve important properties of turbulence,

and that we will use as a guide when we investigate the effects of rotation and magnetic field on turbulence. It consists in plotting the time-scale τ of the relevant physical phenomena as a function of their length-scale ℓ.

Figure 3 shows $\tau(\ell)$ versus ℓ for classical hydrodynamic Kolmogorov turbulence, in a log-log plot. For the sake of illustration, we have assumed that energy is injected at the integral scale ($\ell = r_o$) at a typical time-scale $t_{SV} = 300$ years for flow in the core at this length scale. Let us draw the relevant $\tau_u(\ell)$ turnover time of an eddy of radius ℓ. In Kolmogorov's universal turbulence with its $E(k) \simeq \epsilon^{2/3}k^{-5/3}$ energy density spectrum, the typical eddy turnover time is given by:

$$\tau_u(\ell) \simeq \ell^{2/3}\epsilon^{-1/3}, \tag{18}$$

since $E(k)k \simeq u^2(\ell)$ and[1] $k \sim 1/\ell$.

When eddy turnover times are shorter than viscous diffusion time at the same ℓ, fluid motions follow Kolmogorov's cascade downscale until the $\tau_u(\ell)$ line intersects the viscous time line. Intersection points in NS-regime diagrams correspond to scales at which the regime changes. This intersection corresponds to $\mathrm{Re}(\ell) = u(\ell)\ell/\nu \sim 1$, where $\mathrm{Re}(\ell)$ is the ℓ-scale Reynolds number, hence the scale at which the regime changes from the inertial range to the diffusive range.

The energy dissipation per unit mass ϵ is simply deduced from the ratio of the kinetic energy (per unit mass) at this scale divided by the corresponding time-scale, yielding $\epsilon = \ell^2/\tau_\nu^3(\ell) = \nu/\tau_\nu^2(\ell)$. Multiplying by the mass of the liquid outer core $M_o = 1.835 \times 10^{24}$ kg, we obtain the total viscous dissipation, which we have indicated by squares along the $\tau_\nu(\ell)$ viscous line. The squares are a factor 10^3 apart, and the TW square (1 TW = 10^{12} W) is filled for reference.

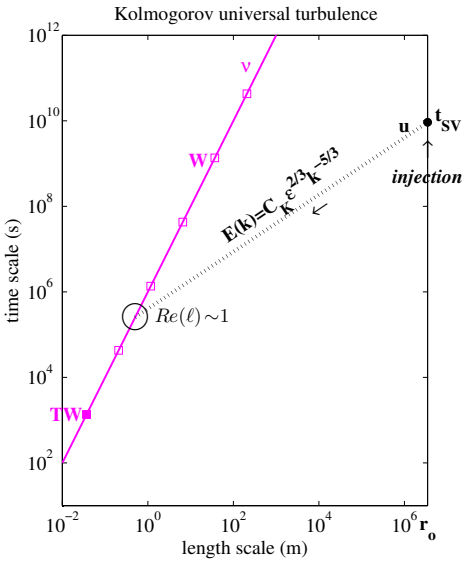

Figure 3: NS-regime diagram (or $\tau-\ell$ diagram) for Kolmogorov's universal hydrodynamic turbulence. Energy cascades from the injection scale (taken here as the integral scale $\ell = r_o$ with time-scale $t_{SV} = 300$ years) following Kolmogorov's universal law $\tau_u(\ell) = \ell^{2/3}\epsilon^{-1/3}$ down to the dissipation scale when it intersects the viscous line $\tau_\nu(\ell)$, yielding $\mathrm{Re}(\ell) \sim 1$. Viscous dissipation can be read at this intersection point, using values graduated along the $\tau_\nu(\ell)$ line.

8.2. Turbulent convection and the Rayleigh number

Convective motions appear in a fluid layer heated at the bottom and cooled at the top when the temperature gradient is large enough.

8.2.1. The Rayleigh number

Lord Rayleigh established that the onset of convection is attained when the Rayleigh number Ra_0 reaches a critical value Ra_c, where the Rayleigh number (at the integral scale) is defined as:

$$\mathrm{Ra}_0 = \frac{(-\Delta\rho/\rho)g r_o^3}{\kappa\nu}, \tag{19}$$

with r_o the thickness of the fluid layer, g the acceleration due to gravity, κ the thermal diffusivity of the fluid and ν its kinematic viscosity. The $-\Delta\rho/\rho$ term determines the relative density ratio across the layer. It is equal to $\alpha\Delta T$ when the density variations are due to temperature alone, where α is thermal expansivity and ΔT the temperature variation.

It is not so easy to estimate the Rayleigh number in the liquid core, because most of the temperature contrast between the top of the core and its base is due to compression via the equation of state (see the Overview Chapter by Olson (2015)). This part defines the adiabatic (or isentropic) temperature profile, and only the density variations in excess of it should be included in the $\Delta\rho$ term in the expression of the Rayleigh number. Since heat conducted along the adiabat is large, it is possible that the Rayleigh number is sub-critical in part of the core. However, as soon as the density profile departs from the adiabat, the Rayleigh number can get very large.

We will use the NS-regime diagram of figure 4 to illustrate this point. One can define a ℓ-scale **Rayleigh number** $\mathrm{Ra}(\ell)$ as a thermal diffusion time $\tau_\kappa(\ell)$ times a viscous diffusion time $\tau_\nu(\ell)$ divided by the square of a

[1] note that in this Chapter we will occasionally drop 2π factors and other pre-factors for simplicity, since we are mainly dealing with orders of magnitude

property	value	unit	description
κ	$5\ 10^{-6}$	$m^2 s^{-1}$	thermal diffusivity
D	10^{-9}	$m^2 s^{-1}$	chemical diffusivity
ν	10^{-6}	$m^2 s^{-1}$	kinematic viscosity
η	1	$m^2 s^{-1}$	magnetic diffusivity
r_o	$3.48\ 10^6$	m	radius of the core
M_o	$1.835\ 10^{24}$	kg	mass of the outer core
t_Ω	$1.38\ 10^4$	s	rotation time of the Earth (*i.e.* $1/2\pi$ day)
t_{SV}	$9\ 10^9$	s	r_o-scale core flow time from secular variation inversion (*i.e.* $\simeq$ 300 years)
t_{Alfven}	$1.4\ 10^8$	s	r_o-scale torsional Alfvén wave time (*i.e.* $\simeq$ 4 years)
$\mathcal{P}$	$< 10^{13}$	W	power dissipated in the core

Table 3: Properties of the core with their numerical values used to draw the figures, as gathered by Olson (2015) in the Overview Chapter). Note that some properties have large uncertainties (see Overview Chapter). We also define the spin-up time $t_{spin-up} = r_o/\sqrt{\nu\Omega} \simeq 13\,000$ years.

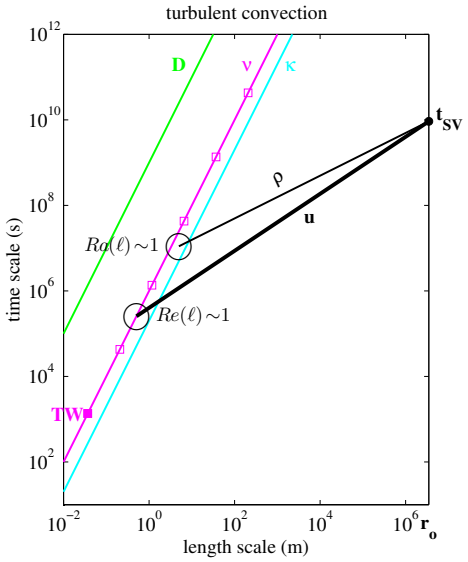

Figure 4: NS-regime diagram for turbulent thermal convection. The intersection of the 'buoyancy' line $\tau_\rho(\ell)$ with a line at mid-distance between the viscous line $\tau_\nu(\ell)$ and the thermal diffusion line $\tau_\kappa(\ell)$ defines $Ra(\ell) \sim 1$, where the regime changes from convective at larger scales to diffusive at smaller scales. The $\tau_u(\ell)$ line gives the evolution of the eddy turnover time as a function of ℓ, and is here assumed to follow Kolmogorov's law from the integral scale ($\tau_u(r_o) = t_{SV}$) down to the diffusion scale, where the $\tau_u(\ell)$ line intersects the $\tau_\nu(\ell)$ line, yielding $\mathrm{Re}(\ell) \sim 1$.

'buoyancy time' $\tau_\rho(\ell)$ (which is analogous to the inverse of the buoyancy frequency used in stratified fluids):

$$\mathrm{Ra}(\ell) = \frac{\tau_\kappa(\ell)\,\tau_\nu(\ell)}{\tau_\rho^2(\ell)}, \qquad (20)$$

where $\tau_\rho(\ell) = \sqrt{\frac{\ell}{g}\frac{\rho}{|\Delta\rho|}}$, $\tau_\kappa(\ell) = \ell^2/\kappa$ and $\tau_\nu(\ell) = \ell^2/\nu$. Using the diffusivities listed in the Overview Chapter by (Olson, 2015) and given again in Table 3, we trace the lines defined by $\tau_\kappa(\ell)$ and $\tau_\nu(\ell)$ in figure 4.

8.2.2. Density perturbation

All we know from observations about density perturbations $\Delta\rho/\rho$ is that they are too small to be detected. We pick here a value $\Delta\rho/\rho \simeq 10^{-15}$, which we will justify below, to trace $\tau_\rho(\ell)$. Where $\tau_\rho(\ell)$ is half-way between $\tau_\kappa(\ell)$ and $\tau_\nu(\ell)$ defines the length-scale ℓ and corresponding timescale at which $\mathrm{Ra}(\ell) \sim 1$. Buoyant fluid parcels with dimensions larger than a few meters will rise with typical rise time of several months. We have also drawn the line $\tau_D(\ell)$ that corresponds to chemical diffusion. We see that chemical (or compositional) convection would start for smaller fluid parcels.

We will see later, when we introduce the role of rotation, that a better value for $\Delta\rho/\rho$ is probably about 10^{-9}. The present value was chosen to be consistent with the hypothesis that large-scale core motions were due to thermal convection, in the absence of rotation and magnetic field. One may then relate the large-scale time t_{SV} to the integral Rayleigh number Ra_0 and thus deduce $\Delta\rho/\rho$. The scaling law for convective large scale velocity U is not that well known. An *ad hoc* scaling such as $U \simeq \mathrm{Ra}_0^{1/2}\sqrt{\kappa\nu}/r_o$ is not unreasonable in our range of Prandtl and Rayleigh numbers (see Ahlers et al. (2009) for a review) and simply yields $\Delta\rho/\rho \simeq r_o/gt_{SV}^2 \sim 10^{-15}$ and $Ra_0 \simeq \tau_\kappa(r_o)\,\tau_\nu(r_o)/t_{SV}^2 \sim 10^{17}$.

8.2.3. Injection and dissipation scales

One could think that the scale ℓ at which $\mathrm{Ra}(\ell) \sim 1$ should be the injection scale, in the language of hydrodynamic turbulence. This is not the case in non-rotating convection. Instead, the size of the container appears to be the relevant injection scale, from which energy cascades down to the dissipation scale. More precisely, the classical $k^{-5/3}$ law is retrieved below what is called the Bolgiano scale (after Bolgiano (1959)). The Bolgiano scale appears to be the height of the container in incompressible fluids (Boffetta et al., 2012; Niemela et al., 2000), and the so-called 'scale-height' in compressible fluids when the Rayleigh number Ra_0 is larger than 10^{11} (Rieutord and Rincon, 2010). The scale height $H = C_p/\alpha g$ is the height over which density has changed by a factor e under the effect of pressure. In the core, $H \simeq 8\,900$ km, which is larger than the radius of the core. Therefore the Bolgiano scale should simply be the radius of the core.

We can then estimate what would be the energy spectrum in the core, if the Earth was not rotating and non-magnetic. In the NS-regime diagram of figure 4 we start from the observed large-scale flow t_{SV} at $\ell = r_o$ and cascade following Kolmogorov's law down to the dissipation scale when the $\tau_u(\ell)$ line intersects the viscous line $\tau_\nu(\ell)$. This happens at a Kolmogorov length-scale of about 1 m. We deduce the dissipation per unit mass $\epsilon = \ell^2/\tau_\nu^3(\ell) = \nu/\tau_\nu^2(\ell) \sim 10^{-17}$ W/kg, which yields a total viscous dissipation of about 30 MW only.

The idea that buoyancy, which is the driving force of the geodynamo, is available to produce turbulent motions within the core without impeding a specific scale is important to keep in mind.

8.3. Turbulence in a rotating sphere

We have seen in previous Chapters that global rotation imposes strong constraints upon flow structures. The Taylor-Proudman theorem implies that the axes of the turbulent eddies are essentially aligned with the axis of rotation of the rotating container. This has lead to the idea that turbulence in rotating fluids is essentially two-dimensional. Enabling high-resolution numerical simulations (e.g. Legras et al., 1988) and powerful statistical mechanics approaches (Robert and Sommeria, 1991), 2D-turbulence has been intensively studied early on (Kraichnan and Montgomery, 1980). In the absence of dissipation and forcing, two-dimensionality results in the conservation of the total enstrophy (the integral of the squared vorticity $\int \omega^2$), thereby modifying the classical Kolmogorov cascade into a double cascade: an inverse cascade of energy from the injection scale up to larger length-scales with a spectral energy density spectrum $E(k) \sim k^{-5/3}$, and a direct cascade of enstrophy from the injection scale down to smaller length-scales with $E(k) \sim k^{-3}$.

However, in a layer at the surface of a rotating sphere, such as the atmosphere, there is an essential difference: strong zonal motions can appear, which are fed by the eddies. Indeed, vortices that move away from the axis of rotation experience a reduction of the Coriolis force, which vanishes at the equator. This limits the extent of eddies in a latitudinal direction and leads to quasi-geostrophic vortices. On the contrary, azimuthal velocities, which follow geostrophic contours, encounter no resistance, except for viscous friction in the Ekman layers that form at the boundary. These phenomena are nicely displayed in the atmosphere of giant planets, such as Jupiter and Saturn, where strong alternating azimuthal jets circle the planet, entraining and shearing quasi-geostrophic vortices.

Similarly, in a thick layer such as the liquid outer core, columnar vortices that move away from the axis of rotation impinge on the bounding spherical shell. There, the non-penetration condition implies that the velocity component aligned with the cylindrical radius coordinate must convert into a velocity component aligned with the rotation axis, plunging toward the equator from both sides. Such a flow violates the Taylor-Proudman theorem, and is therefore inhibited, while azimuthal (zonal) flows are not affected.

Let us examine the NS-regime diagram of figure 5 to get a sense of the modifications brought up by rotation in the context of core turbulence. One new time-scale stands out: the rotation time of the Earth t_Ω (*i.e.,* $1/2\pi$ day). The intersection of the $\tau_\nu(\ell)$ viscous line with t_Ω defines the thickness of the Ekman layer $\delta_E = \sqrt{\nu/\Omega}$, where Ω is the angular velocity of the Earth. The Ekman layer is about 0.1 m thick. We also introduce the spin-up time $t_{spin-up} = r_o/\sqrt{\nu\Omega} \simeq 13\,000$ years and draw it in figure 5. The spin-up time is the time it takes for the core to adjust to a change in the angular velocity of the mantle through viscous coupling, *i.e.* the time it takes for the whole fluid to circulate through the Ekman layer.

8.3.1. Bidimensionalization and Rossby waves

Inertial waves have periods longer than half-a-day. They are responsible for implementing the Taylor-Proudman constraint on the flows. Flows at timescales shorter than half-a-day will not be bidimensionalized. In fact, a blob of vorticity of size ℓ grows into a bidimensional column at a speed equal to $\Omega\ell$ (Davidson, 2013). This means that it takes only a few days for such a blob to convert into an elongated vorticity column, say

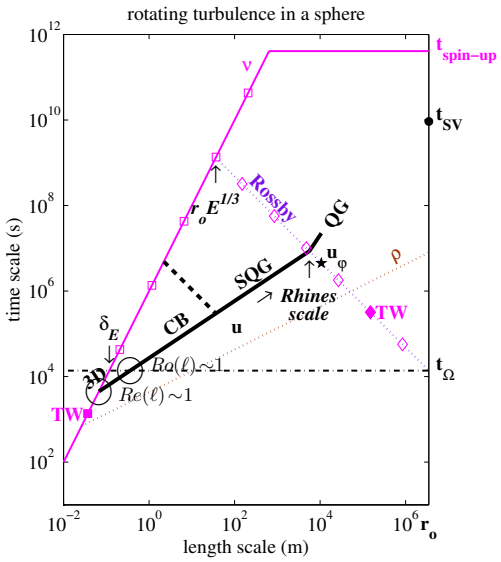

Figure 5: NS-regime diagram for rotating turbulence in a spherical shell. Rotation yields a specific time scale: t_Ω (dash-dot horizontal line). Its intersection with the viscous line (magenta) yields the Ekman boundary layer thickness δ_E. We also draw a horizontal line for the spin-up time $t_{spin-up} = r_o/\sqrt{\nu\Omega}$. The dotted line labeled 'Rossby' represents the time $\tau_{Rossby}(\ell)$ it takes for a Rossby wave to propagate one wavelength ℓ. Its intersection with the viscous line occurs for $\ell = r_o E^{1/3}$, which is the width of convective columns at the onset of convection. The brown dotted line labeled ρ represents the buoyancy line $\tau_\rho(\ell)$. The u_φ star on the Rossby line marks the width (Rhines scale) and velocity of the zonal jets that would make a turn round the Earth in time t_{SV}. The black solid line is the eddy turnover time $\tau_u(\ell)$ line of non-zonal eddies that we infer, starting from the Rhines scale in the quasi-geostrophic (QG) regime. It becomes semi-quasi-geostrophic (SQG) and follows Kolmogorov's slope after crossing the Rossby line, and might enter critical balance (CB) at scales smaller than the injection scale (here taken as $r_o E^{1/3}$). The intersection with t_Ω defines $Ro(\ell) \sim 1$. Turbulence becomes three-dimensional (3D) below the t_Ω line. The intersection with the viscous line defines $\mathrm{Re}(\ell) \sim 1$ and provides the amount of viscous dissipation. Viscous dissipation of the zonal and quasi-geostrophic flows occurs in the Ekman layers and is read on the Rossby line, where diamonds are a factor 10^3 apart, and the TeraWatt diamond is filled for reference.

ten times longer than wide, whatever the value of ℓ. In a thin layer such as the atmosphere or the ocean, the columns rapidly extend across the entire layer.

However, it is important to realize that in a thick layer such as the liquid outer core, the time required for such a column to reach the core-mantle boundary is given by $\tau_{Rossby}(\ell) = r_o/\Omega\ell$. The corresponding line is drawn if figure 5. We have labelled it as the Rossby line, because it also roughly corresponds to the time it takes for a Rossby wave of azimuthal wavelength ℓ to propagate one wavelength. Indeed, the expression of the pulsation of a Rossby wave, as recalled in Chapter by Jault and Finlay (2015) reads:

$$\omega_{Rossby} = -2\Omega\frac{\beta k_\varphi}{k^2},$$

with $\beta = \alpha/H_c$, where α is the slope of the spherical shell and H_c the height of the quasi-geostrophic column, and k is the wavenumber of the Rossby wave. Approximating $\alpha \sim 1$ and $H_c \sim r_o$ at mid-latitudes, and $k \sim k_\varphi$, we retrieve $\tau_{Rossby}(\ell) \sim r_o/\Omega\ell$.

Above the Rossby line, columns extend across the entire core: motions are quasi-gesostrophic (QG). Assuming that ℓ now defines the diameter of the columnar eddies in the equatorial plane, the viscous line $\tau_\nu(\ell)$ is unchanged. However, viscous friction is also present at the ends of the column. There, the velocity drops to zero at the rigid core-mantle boundary. The velocity drop takes place across an Ekman layer of thickness δ_E thin enough for viscous forces to balance the Coriolis force. The dissipation per unit mass due to viscous friction at the ends of the columns can be written:

$$\epsilon_{QG} = \frac{\ell^2}{\tau_u^2(\ell)\, t_{spin-up}}. \qquad (21)$$

The intersection of the viscous line $\tau_\nu(\ell)$ with the spin-up time marks the length scale at which friction on the walls of a column equal friction at its ends. It occurs for a length $\ell = r_o \mathrm{E}_0^{1/4}$, where $\mathrm{E}_0 = \nu/\Omega r_o$ is the Ekman number at the integral scale.

We expect that turbulent motions whose time- and length-scales fall in the triangle bounded by the three lines t_Ω-τ_ν-τ_{Rossby} will be strongly influenced by rotation with elongated eddies aligned with the rotation axis (z-axis). Those above the $\tau_{Rossby}(\ell)$ line will be quasi-gesotrophic (QG) columnar vortices extending all the way across the liquid core. We find it logical to evaluate on the Rossby line the viscous dissipation due to quasi-geostrophic and zonal motions since below this line, columns will not necessarily reach the surface Ekman layers. QG and zonal flow viscous dissipation $M_o\epsilon_{QG}$ is

thus graduated with diamonds on the Rossby line. The diamonds are a factor 10^3 apart, and the TW diamond (1 TW = 10^{12} W) is filled for reference.

8.3.2. Zonal flows and potential vorticity

We have seen that truly geostrophic motions (*i.e.* zonal (or azimuthal) motions in a sphere or a spheroid) behave in a specific way. In contrast to non-axisymmetric motions, they get organized in winds or jets of a given width. Their lifetime can be extremely long, and they often carry the largest part of the kinetic energy of the flow. Clearly, these bands will limit the maximum size that QG-columns can achieve, since they are separated by what appears to be strong barriers. There has been much debate on the origin and characteristics of these bands. One idea has become quite successful, which assess that bands are the expression of the mixing of potential vorticity (PV) in a staircase fashion (Dritschel and McIntyre, 2008). Potential vorticity q defined by $q = (\omega_z + 2\Omega)/H_c$ is an important quantity in rotating fluids because it is conserved when advected by a columnar flow (ω_z being the z-component of the vorticity in the rotating frame, and H_c the height of the column), when viscous effects are ignored. In a stratified medium with linear density profile, mixing produces a stack of layers in which the density is fairly homogeneous, and which remain isolated from each other because the sharp density jump across their borders acts as a barrier for small density fluctuations (Phillips, 1972). It is believed that something very similar happens for potential vorticity in a rotating fluid in a sphere.

The conservation of potential vorticity is also at the origin of Rossby waves. As a column of fluid at rest (outside the cylinder tangent to the inner core) moves away toward the mantle, its height decreases. In order to conserve potential vorticity, the column acquires a negative vorticity (in the rotating frame). The opposite holds for a column moving towards high latitude. Both contribute to a prograde, *i.e.,* eastward, motion. This wave motion is called a Rossby wave. Note that in shallow layers such as ocean or atmosphere at the surface of a rotating planet, Rossby waves propagate westwards because the planetary vorticity gradient has the opposite sign. The velocity of Rossby waves increases when their wave number decreases. We have drawn the line $\tau_{Rossby} = r_o/\Omega\ell$ as representing the time scale *versus* length scale signature of Rossby waves in the NS-regime diagram of figure 5.

The intersection of the Rossby line $\tau_{Rossby}(\ell)$ with the eddy turnover time $\tau_u(\ell)$ defines a Rhines length scale ℓ_{Rhines} while its intersection with the viscous line $\tau_\nu(\ell)$ provides the length scale of thermal Rossby waves $r_o E_0^{1/3}$, which appear at the threshold of convection (Busse, 1970; Jones et al., 2000). The Rhines scale describes how the sphericity of the core stops the inverse cascade of energy from small scale vortices.

8.3.3. Possible turbulent regimes

Let us now try to infer what would be the different turbulent regimes encountered in the core if it was non-magnetic but rotating. Starting from the 'observed' time scale t_{SV} at the largest length scale r_o, we run into a problem: there should be no motion at this scale, since the maximum diameter of columnar eddies is set by the width of zonal bands. We should therefore re-interpret t_{SV} as the typical time a zonal jet takes to circle once around the core. This sets its velocity $u_\varphi = 2\pi r_o/t_{SV}$, which enters the definition of the Rhines scale: $\ell_{Rhines} \sim \sqrt{u_\varphi r_o/\Omega}$ (Dritschel and McIntyre, 2008). We assume that this defines the width of the zonal jets. The corresponding viscous dissipation can be read on the Rossby line. Guided by observations of the atmosphere of Jupiter, we further assume that the velocity of the eddies at the same scale (their maximum size) will be five times smaller, thus defining the starting point of the turbulent regime diagram we want to construct. Note that actual large-scale zonal velocities are similar to non-zonal velocities in the Earth's core (Hulot et al., 2002; Pais and Jault, 2008) (see Chapter by Holme (2015)).

Above the Rossby line, these eddies are columns extending all the way across the core. The dissipation of these QG-vortices can be read at the intersection of the $\tau_u(\ell)$ line with the Rossby line. It is always smaller than that of the zonal jets (because we have assumed eddies have smaller velocities than jets). The inverse energy cascade yields a Kolmogorov-like law for $\tau_u(\ell)$ in that regime. Below the Rossby line, vortices are still very much elongated in the z-direction, but they do not necessarily extend all the way across the core. We label this regime SQG for semi-quasi-geostrophic. In 2D-turbulence, the conservation of enstrophy modifies the turbulent cascade: energy cascades from the injection scale upscale to the largest possible scale (the inverse energy cascade), while enstrophy cascades downscale.

8.3.4. Below the injection scale

What is the injection scale in our case? Near the onset of convection, it would be the length scale of thermal Rossby waves $r_o E_0^{1/3}$ (Busse, 1970). However, when strong zonal winds are present, they certainly inject energy and enstrophy at their (larger) scale. 2D-turbulence scenarios as well as quasi-geostrophic numerical models predict a strong decrease of energy for scales below the injection scale. The thick dashed line in fig-

ure 5 displays what would be the τ_u line in the case of an energy spectrum $E(k) \sim k^{-5}$. However, we have seen that rotating turbulence was not strictly 2D in this regime (below the Rossby line). It has been recently proposed by Nazarenko and Schekochihin (2011) that the flow reaches a 'critical balance' (CB) in this regime that sees the columns progressively shrink in length until 3D-turbulence is reached at $Ro(\ell) \sim 1$ (at the intersection of the $\tau_u(\ell)$ and t_Ω lines). This is what we have drawn in figure 5, keeping the Kolmogorov slope all the way down to the dissipation scale ($\mathrm{Re}(\ell) \sim 1$), where the remaining viscous dissipation can be read.

Note that in our scenario, the $\tau_u(\ell)$ line barely gets below t_Ω, meaning that turbulence remains influenced by rotation almost down to the dissipation scale. Also note that the total viscous dissipation (zonal and QG plus SQG) is now of the order of 100 GW, compared to 30 MW in the absence of rotation. As rotation inhibits convection, a larger energy input and larger buoyancy forces are needed to provide the velocities we observe. The $\Delta\rho/\rho$ term can be estimated here by assuming a balance between the buoyancy and the Coriolis forces yielding: $\Delta\rho/\rho \simeq 2\Omega r_o/g\, t_{SV} \sim 10^{-9}$, some six orders of magnitude larger than in the non-rotating case. Hence the position of the $\tau_\rho(\ell)$ line in figure 5.

8.4. MHD turbulence

Let us pursue our exercise by building a plausible scenario of turbulence if the core had the magnetic field we observe at large scales but was not rotating.

8.4.1. Mechanisms of MHD turbulence

Turbulence in the presence of a strong imposed magnetic field is quite different from classical hydrodynamic turbulence. While eddies are the building bricks of hydrodynamic turbulence, it is believed that Alfvén waves are those of magnetohydrodynamic turbulence (Tobias et al., 2013), at least as long as fluid velocities are smaller than the Alfvén speed ($u(l) < V_A$) and the Lundquist number is large $Lu(\ell) \gg 1$. In a uniform magnetic field, these waves are non-dispersive so that wave-packets of any shape propagate without distortion. However, the collision of counter-propagating Alfvén waves do produce some distortion as the waves then propagate along modified field lines. These collisions produce smaller scales to which energy cascades down without dissipation, just like in classical hydrodynamic turbulence, until the dissipation scale is reached. Indeed, the half sum and half difference of the energies E^+ and E^- of the Elsasser variables correspond, respectively, to the total energy and cross-helicity $\int \boldsymbol{u}\cdot\boldsymbol{b}$, which are both conserved in ideal incompressible MHD.

Two regimes have been identified: weak turbulence, in which the linear term $(\boldsymbol{V}_A\cdot\boldsymbol{\nabla})\,z^\pm$ of equation 17 dominates over the non-linear term $(z^\mp\cdot\boldsymbol{\nabla})\,z^\pm$, and strong turbulence when the opposite holds. In weak turbulence, it takes several collisions of wave packets for energy to cascade to smaller scales and the energy spectral density is inferred to scale as $E(k) \sim k^{-2}$, while non-linear collisions in strong turbulence are more efficient in that respect, yielding $E(k) \sim k^{-3/2}$. The transition occurs when the Alfvén wave collision time $\tau_b(\ell)$ is of the same order as the large-scale Alfvén wave time t_{Alfven}. Turbulence always gets strong at short length-scales. Note that in both cases, one expects an equipartition of energy between the velocity and magnetic fluctuations since Alfvén waves are in equipartition. It is also important to realize that the cascade is for length-scales perpendicular to the direction of the guide field $\boldsymbol{B}_0$: the wave packets retain their along-field shape. As a consequence, the wave packets become more and more elongated in the guide field direction, somewhat like vortices are elongated along the rotation axis in rotating turbulence, except that the effect gets larger as the length-scale gets smaller, in contrast to the rotating case.

8.4.2. Two scenarios of MHD turbulence

Let us try to sketch the turbulent regimes a magnetized non-rotating Earth would experience. We will discuss two alternative scenarios and use the NS-regime diagrams of figure 6 and 7 as a guide. We again consider that we know the values of the diffusivities, and draw a new line for magnetic diffusion as $\tau_\eta(\ell) = \ell^2/\eta$. The large-scale starting point for the velocity field is the same as before, deduced from secular variation core flow inversion. We also assume that we know the intensity of the large-scale magnetic field. Indeed, the recent discovery of torsional waves in the Earth's core (Gillet et al., 2010) provides a profile of the *rms* intensity of the s-component of the magnetic field as a function of s, where s is the cylindrical radius.

We infer a typical intensity of $B_0 = 3$ mT, which translates into a large-scale Alfvén wave velocity $V_A = B_0/\sqrt{\rho\mu_0} \simeq 25$ mm/s. Note that in fact, the velocity of torsional oscillations depends upon the integral of B_s^2 over azimuth and z, so that the contribution of small-scales is included in our estimate of B_0. We plot the line $\tau_{Alfven} = V_A\ell$ in the NS-regime diagram of figure 6. At the largest scale ($\ell = r_o$), the corresponding time is about 10^8s, that is a few years, some two orders of magnitude smaller that the characteristic time of secular variation. This is just an expression of the fact that magnetic energy is about four orders of magnitude larger than kinetic energy in the Earth's core. In-

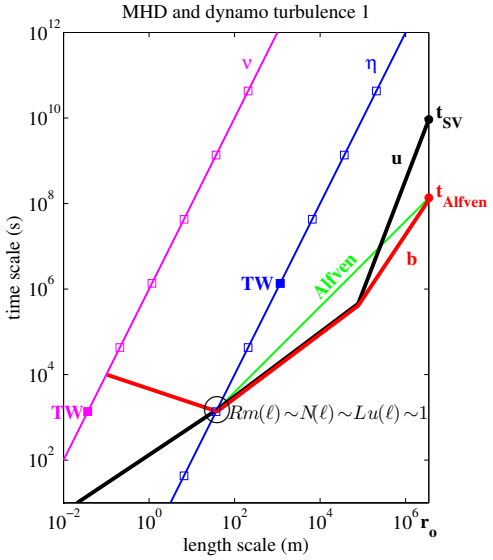

Figure 6: A highly dissipative scenario for magnetohydrodynamic and dynamo turbulence. The time-scale of the large-scale magnetic field is t_{Alfven}, deduced from the velocity V_A of torsional oscillations. The green line $\tau_{Alfven}(\ell)$ gives the time it takes for an Alfvén wave to travel a distance ℓ at this velocity V_A. The red line $\tau_b(\ell)$ measures the strength of the magnetic field at length-scale ℓ: it is the characteristic collision time of Alfvén waves. The blue line $\tau_\eta(\ell)$ is the magnetic diffusion line. Ohmic dissipation is graduated with squares along that line. The squares are a factor 10^3 apart, and the TW square is filled. Here, we assume that the τ_u, τ_b and τ_{Alfven} lines all intersect the τ_η line at the same point, where $\mathrm{Rm}(\ell) \sim N(\ell) \sim \mathrm{Lu}(\ell) \sim 1$, yielding unrealistic ohmic dissipation of millions of TW. The eddy turnover time τ_u continues downscale and intersects the τ_ν line at very small scales, yielding again unrealistic viscous dissipation. This scenario is discarded because it would imply super-alfvenic velocities.

deed, when expressed in Alfvén velocity, the magnetic field intensity directly compares to flow velocity. The intersection of the $\tau_\eta(\ell)$ and $\tau_{Alfven}(\ell)$ lines defines the minimum wavelength ℓ Alfvén waves can achieve without being completely dissipated. It corresponds to an ℓ-scale Lundquist number $\mathrm{Lu}(\ell) = \tau_\eta(\ell)/\tau_{Alfven}(\ell) \sim 1$.

Where should we plot the lines for the typical velocity field $\tau_u(\ell)$ and for the line for typical magnetic field $\tau_b(\ell)$ (expressed in Alfvén wave time) ? We apply the principles of the MHD turbulence cascade we just described. Assuming equipartition down to the magnetic diffusion scale implies that both the $\tau_u(\ell)$ and $\tau_b(\ell)$ lines should intersect the $\tau_\eta(\ell)$ magnetic diffusion line at the same place in the diagram, which will thus correspond to $\mathrm{Rm}(\ell) \sim 1$.

8.4.3. A highly dissipative scenario

It is then tempting to infer that smaller scales will be in a regime where the small-scale magnetic field results from the diffusion of the magnetic field induced by the interaction of the small-scale velocity field with the large-scale magnetic field. In this diffusive regime, one has: $(\boldsymbol{B}_0 \cdot \boldsymbol{\nabla})\boldsymbol{u} \sim \eta \nabla^2 \boldsymbol{b}$, yielding $b \sim uB_0\ell/\eta$, which translates into: $\tau_b(\ell) = \tau_{Alfven}(\ell)\,\tau_u(\ell)/\tau_\eta(\ell)$. Since we defined the intersection point by $\tau_u(\ell) = \tau_b(\ell) = \tau_\eta(\ell)$, the intersection should take place where the $\tau_\eta(\ell)$ and $\tau_{Alfven}(\ell)$ lines intersect. This intersection thus simultaneously correspond to $\mathrm{Lu}(\ell) \sim 1$, $\mathrm{Rm}(\ell) \sim 1$ and $\mathrm{N}(\ell) \sim 1$, where $\mathrm{N}(\ell)$ is the ℓ-scale interaction parameter that measures the effect of the large-scale magnetic field on the velocity field.

At this intersection point, magnetic diffusion takes over and we read the Ohmic dissipation ($= M_o\eta/\tau_\eta^2(\ell)$) on the $\tau_\eta(\ell)$ line. It reaches a million TeraWatts, a value that is clearly unacceptable since no core flux can be larger than our estimate of a total flux from the mantle to the core of 13 TW (see Table 3). The velocity field is probably reduced at this intersection, but what remains should still cascade downscale (Plunian et al., 2013). One can easily check that the interaction parameter decreases as the length scale decreases in this regime, so that hydrodynamic turbulence is recovered with its classical Kolmogorov cascade, as drawn. Figure 6 shows that we finally reach the viscous line $\tau_\nu(\ell)$ for length scales below a millimeter, and read a viscous dissipation of a million TeraWatts again!

There is one problem with this scenario. MHD turbulence above the intersection point at $\mathrm{Rm}(\ell) \sim 1$ would be in the strong turbulence regime, for which the energy spectrum is found to be $E(k) \sim k^{-3/2}$ (Tobias et al., 2013), yielding $\tau \sim \ell^{3/4}$, as drawn in figure 6. This means that the $\tau_u(\ell)$ line is *below* the $\tau_{Alfven}(\ell)$ line over

a large range of scales, implying that the fluid velocity is larger than the Alfvén speed, which contradicts the hypotheses of Alfvén wave turbulence.

8.4.4. *A more realistic scenario*

We thus take into account the latter constraint and require that τ_u and τ_b remain above the Alfvén line. The new scenario we build is drawn in figure 7. We let the MHD strong turbulence cascade start from the largest scale r_o at time t_{Alfven}, and assume it goes all the way down to the length-scale $\ell \sim \eta \sqrt{\rho\mu_0}/B_0$ for which $Lu(\ell) \sim 1$, at the intersection of the $\tau_\eta(\ell)$ and $\tau_{Alfven}(\ell)$ lines. Equipartition is still required, implying that $\tau_u(\ell)$ gets down to times much shorter than t_{SV} to join the $\tau_b(\ell)$ line. We have assumed here a spectrum $E_u(k) \sim k$ for this part, meaning that there is more kinetic energy at small scale than at the integral scale. In contrast with the previous scenario, the interaction parameter $N(\ell) = \tau_u^2(\ell)/\tau_{Alfven}(\ell)\,\tau_b(\ell)$ remains large at all scales, meaning that the large-scale magnetic field strongly influences the flow. Turbulence in the magnetic diffusive regime with a strong applied magnetic field has been explored in laboratory experiments (Alemany et al., 1979). The small-scales of the flow are severely damped by the applied magnetic field: the kinetic energy spectrum is $E_u(k) \sim k^{-3}$, which translates into a constant $\tau_u(\ell)$, as drawn in figure 7. The magnetic energy spectrum is even steeper (not drawn), obeying the induction-diffusion balance. We read an Ohmic dissipation of more than a thousand TeraWatts, which could be much lower though if the strong MHD turbulence spectrum was steeper than $k^{-3/2}$.

Assuming equipartition at small scale down to the magnetic diffusion scale has a drastic influence on the kinetic and magnetic energy spectra. It is difficult to build scenarios that do not require an unrealistic ohmic dissipation. We will see that rotation can help us recover a more viable scenario.

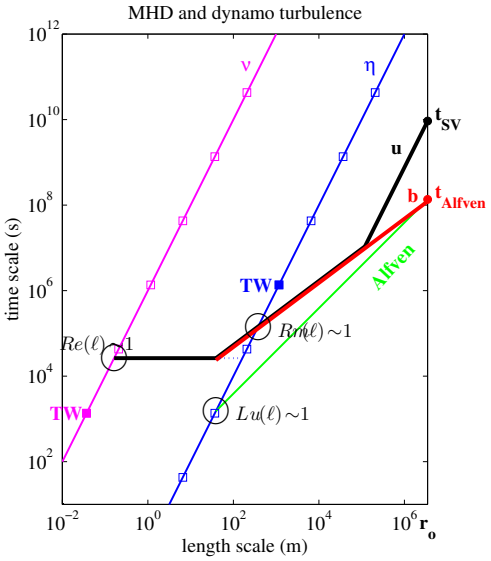

Figure 7: A more realistic scenario for magnetohydrodynamic and dynamo turbulence. In this scenario, we relax the hypothesis that the induction-diffusion balance is achieved at Rm $\sim$ 1. Instead, we consider than Alfvén waves can propagate down to a scale ℓ where $Lu(\ell) \sim 1$, *i.e.* at the intersection of the $\tau_\eta(\ell)$ line (blue) with the $\tau_{Alfven}(\ell)$ line (green). We assume that the strong turbulence MHD cascade begins at the largest scale r_o. The interaction parameter $N(\ell)$ remains large at all scales, and the flow at small scale is strongly damped by the large-scale magnetic field. Projecting along the blue dashed line yields an Ohmic dissipation of about a thousand TeraWatts, as read on the $\tau_\eta(\ell)$ line.

8.5. *Turbulence in planetary cores*

The Earth is rotating rather fast. On periods longer than a day, rotation inhibits Alfvén waves (Braginsky, 1970; Jault, 2008). Only geostrophic Alfvén waves, *i.e.* torsional oscillations, are not inhibited. They have indeed been detected in the core (Gillet et al., 2010), and we have used their observed velocity to set our magnetic time t_{Alfven} at the integral scale r_o. Quasi-geostrophic Alfvén waves are also possible. But in both cases, the constraint of rotation prevents Alfvén wave collision to be the mechanism by which the magnetic energy cascades down to dissipation.

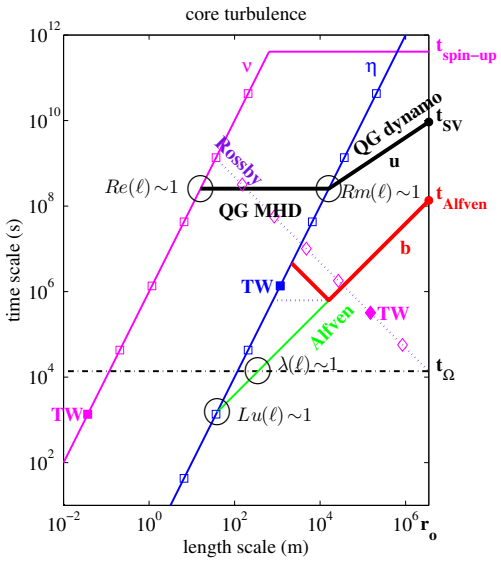

Figure 8: NS-regime diagram for turbulence in the Earth's core. Both rotation and the magnetic field are taken into account, combining the lines already defined in figures 5, 6 and 7. We assume that the kinetic energy density follows a $k^{-5/3}$ law in the quasi-geostrophic dynamo regime. The intersection of the $\tau_u(\ell)$ and $\tau_\eta(\ell)$ lines defines $Rm(\ell) \sim 1$, which marks the transition from the dynamo to the diffusive regime. Quasi-geostrophic (QG) and semi-quasi-geostrophic (SQG) diffusive MHD governs the following part, with a kinetic energy density spectrum in k^{-3} (yielding a flat $\tau_u(\ell)$ line) and a magnetic energy density spectrum in k^{-5}. Viscous dissipations of the QG (read on the Rossby line) and of the SQG (read on the $\tau_\nu(\ell)$ line) MHD flows amount to a few kiloWatt only. Ohmic dissipation is maximum at the length scale ℓ where $\mathrm{Rm}(\ell) \sim 1$. Projecting along the blue dashed line yields an Ohmic dissipation of a few TeraWatt, as read on the $\tau_\eta(\ell)$ line. Alfvén waves can be excited and propagate for scales falling on the Alfvén green line between its intersection with t_Ω (which defines $\lambda(\ell) \sim 1$) and that with the magnetic diffusion line (which defines $Lu(\ell) \sim 1$).

Using the NS-regime diagram of figure 8, let us try to infer what turbulence could look like in the core, taking into account the Earth's rotation, and the presence of a strong large-scale magnetic field. The main difference with the previous scenarios is that we do not impose equipartition at small scales. We let the eddy turnover time $\tau_u(\ell)$ decrease with length-scale ℓ, assuming a spectrum $E_u(k) \sim k^{-5/3}$ in the dynamo regime. The intersection of the $\tau_u(\ell)$ line with $\tau_\eta(\ell)$ defines the length-scale where $\mathrm{Rm}(\ell) \sim 1$, below which the flow cannot generate a magnetic field. Below this scale, if the large-scale magnetic field B_0 is dominant, the small-scale magnetic field is obtained by the balance between induction and diffusion and obeys $\tau_b(\ell) = \tau_{Alfven}(\ell)\,\tau_u(\ell)/\tau_\eta(\ell)$. This time, flow velocities remain much lower than alfvenic speeds. Since $\tau_u(\ell) = \tau_\eta(\ell)$ for $\mathrm{Rm}(\ell) \sim 1$, the small-scale magnetic field at $\mathrm{Rm}(\ell) \sim 1$ must lie on the Alfvén line. For simplicity, we have thus drawn the $\tau_b(\ell)$ line following the Alfvén line in the dynamo regime.

The interaction parameter $N(\ell) = \tau_u^2(\ell)/\tau_{Alfven}(\ell)\,\tau_b(\ell)$ is very large at all scales, meaning that the large-scale magnetic field strongly influences the flow. Below the scale for which $\mathrm{Rm}(\ell) \sim 1$ we thus enter a diffusive regime with a strong applied magnetic field, where Alfvén waves are inhibited by rotation. Following Alemany et al. (1979), we assume a kinetic energy spectrum $E_u(k) \sim k^{-3}$, which translates into a constant $\tau_u(\ell)$, as drawn in figure 8. The magnetic energy spectrum is even steeper, obeying the induction-diffusion balance.

Note that in our scenario, the flow is above the Rossby line in the dynamo regime, hence quasi-geostrophic. Most of the non-dynamo MHD regime lies above the Rossby line, hence being also quasi-geostrophic (QG). Viscous dissipation can be read along the $\tau_{Rossby}(\ell)$ line for the quasi-geostrophic MHD flow and on the $\tau_\nu(\ell)$ line for the semi-quasi-geostrophic MHD motions. Both are very small, below the kW range. Ohmic dissipation dominates, and mostly occurs at the ℓ-scale where $\mathrm{Rm}(\ell) \sim 1$. It can be read along the $\tau_\eta(\ell)$ line, where the dashed blue line intersects, amounting to a few TW for the present scenario.

Behind this scenario is the idea that turbulence is very much hindered under the combined constraints of strong magnetic field and fast rotation. The rotating magnetized spherical Couette flow (DTS) experiment provides evidence for this behaviour (Nataf and Gagnière, 2008). We end up with a very sluggish core, where the smallest eddies are ten meters in diameter, and have turnover times of several years!

Note that the Alfvén line intersects the $\tau_\eta(\ell)$ line be-

low the t_Ω line. This intersection defines $Lu(\ell) \sim 1$, while the intersection of the Alfvén line with the t_Ω line defines $\lambda(\ell) \sim 1$. In that region of the $\tau - \ell$ diagram, it is possible for Alfvén waves to propagate without being hindered by the Earth's rotation (because $\lambda(\ell) > 1$), and without being damped by magnetic diffusion (because $Lu(\ell) > 1$). However, such waves will not be involved in the cascade of energy from large to small scales. Similarly, fluid motions could be excited at timescales shorter than a day (by tides for example), but they are not part of the energy cascade.

9. Summary and perspectives

Early numerical simulations of the geodynamo have demonstrated the crucial role of rotation in the *generation* of the magnetic field. One of our main messages here is that rotation could also play a key role in limiting the *dissipation* of the magnetic field.

Indeed the classical scenario of MHD turbulence in the absence of rotation, based on the collision of Alfvén waves, predicts dissipation rates far too large for the core. The constraints brought by rotation prevent Alfvén waves to be the carriers of turbulence. Instead, turbulence gets organized in quasi-geostrophic eddies, strongly elongated along the rotation axis, and strongly damped by the large-scale magnetic field. We end up with a very sluggish core, in which the smallest eddies are ten meters in diameter and have turnover times of several years. The smallest magnetic field structures are even larger, in the kilometer range but their life time might be much shorter (of the order of months). In this scenario, viscous dissipation is negligible, while Ohmic dissipation is in the TW range. However, one should keep in mind that slightly different scenarios would lead to largely different dissipations.

We note that a planet like Venus, which rotates much more slowly than the Earth (rotation period of 243 days), would not be in this regime, and would not be able to sustain a magnetic field as large as that of the Earth.

The NS-regime diagram (or $\tau - \ell$ diagram) that we introduced is a useful tool for determining the various regimes that can be encountered when going from the large-scales down to the dissipative scales. We hope it can guide the construction of appropriate parametrizations of turbulence in Large Eddy Simulations.

In exploring the various turbulent scenarios, we have noted that key elements were still missing, calling for more experimental and numerical studies. For example, we don't know how to relate quasi-geostrophic and zonal velocities in a convecting sphere. What is the relevant injection scale in these systems? Furthermore, some fundamental differences between the case of the atmosphere of giant planets and that of the core might have been overlooked. Our observation that the time required for a Taylor column to grow and extend across the core is comparable to the propagation time of a Rossby wave questions the validity of quasi-geostrophic modeling of small scales.

MHD and rotating MHD turbulence is even more uncertain. The scenarios we have built are very speculative and await experimental and numerical backing.

What is the prospect of detecting turbulent structures in the core? We have seen that the expected relative density variations are extremely small ($\sim 10^{-9}$), far too small to affect the propagation of seismic waves or the gravity field. However, the velocity of seismic waves can also be modified by rotation, flow velocity and magnetic field. How important are these effects? Our $\tau - \ell$ diagrams can guide us again. Seismic waves in the core have velocities of about 9km/s, yielding a characteristic time of about 400s at the integral scale r_o. Scattering of seismic waves by turbulent structures roughly scale as their time ratio: strong effects occur when times are comparable. In figure 8 we see that the time that gets closest to the seismic time is t_Ω: indeed it is well known that seismic normal modes of the Earth are split by the Coriolis force. The next relevant time is the magnetic Alfvén wave time, but it is already 3 orders of magnitude further away from seismic times, leaving little hope for detection.

acknowledgments

We thank Dan Lathrop for a fruitful review, and Jérôme Noir for spotting an error in an earlier version of our manuscript.

References

Ahlers, G., Grossmann, S., Lohse, D., 2009. Heat transfer and large scale dynamics in turbulent Rayleigh-Benard convection. Reviews of Modern Physics 81, 503–537. doi:10.1103/RevModPhys.81.503.

Alboussiere, T., Cardin, P., Debray, F., La Rizza, P., Masson, J.P., Plunian, F., Ribeiro, A., Schmitt, D., 2011. Experimental evidence of Alfven wave propagation in a Gallium alloy. Phys. Fluids 23. doi:10.1063/1.3633090.

Alboussière, T., Deguen, R., Melzani, M., 2010. Melting-induced stratification above the Earth's inner core due to convective translation. Nature 466, 744–U9. doi:10.1038/nature09257.

Alemany, A., Moreau, R., Sulem, P., Frisch, U., 1979. Influence of an external magnetic field on homogeneous mhd turbulence. Journal de Mécanique 18, 277–313.

Alfvén, H., 1942. Existence of electromagnetic-hydrodynamic waves. Nature 150, 405–406.

Andreev, O., Kolesnikov, Y., Thess, A., 2013. Visualization of the Ludford column. J. Fluid Mech. 721, 438–453. doi:10.1017/jfm.2013.76.

Anselmet, F., Gagne, Y., Hopfinger, E.J., Antonia, R.A., 1984. High-order velocity structure functions in turbulent shear flows. Journal of Fluid Mechanics 140, 63–89. doi:10.1017/S0022112084000513.

Aubert, J., Jung, S., Swinney, H., 2002. Observations of zonal flow created by potential vorticity mixing in a rotating fluid. Geophys. Res. Lett. 29. doi:10.1029/2002GL015422.

Augier, P., Lindborg, E., 2013. A new formulation of the spectral energy budget of the atmosphere, with application to two high-resolution general circulation models. Journal of the Atmospheric Sciences doi:10.1175/JAS-D-12-0281.1.

Baroud, C., Plapp, B., Swinney, H., She, Z., 2003. Scaling in three-dimensional and quasi-two-dimensional rotating turbulent flows. Physics of Fluids 15, 2091–2104. doi:10.1063/1.1577120.

Berhanu, M., Monchaux, R., Fauve, S., Mordant, N., Pétrélis, F., Chiffaudel, A., Daviaud, F., Dubrulle, B., Marié, L., Ravelet, F., Bourgoin, M., Odier, P., Pinton, J.F., Volk, R., 2007. Magnetic field reversals in an experimental turbulent dynamo. Europhys. Lett. 77, 59001–+. doi:10.1209/0295-5075/77/59001.

Boffetta, G., De Lillo, F., Mazzino, A., Musacchio, S., 2012. Bolgiano scale in confined Rayleigh-Taylor turbulence. J. Fluid Mech. 690, 426–440. doi:10.1017/jfm.2011.446.

Bolgiano, Jr., R., 1959. Turbulent spectra in a stably stratified atmosphere. J. Geophys. Res. 64, 2226–2229. doi:10.1029/JZ064i012p02226.

Braginsky, S., 1970. Spectrum of oscillations of the earth's hydromagnetic dynamo. Geomagn. Aeron 10, 221–233.

Braginsky, S., Meytlis, V., 1990. Local turbulence in the earth's core. Geophysical & Astrophysical Fluid Dynamics 55, 71–87.

Brito, D., Alboussière, T., Cardin, P., Gagniére, N., Jault, D., La Rizza, P., Masson, J.P., Nataf, H.C., Schmitt, D., 2011. Zonal shear and super-rotation in a magnetized spherical Couette-flow experiment. Physical Review E 83. doi:10.1103/PhysRevE.83.066310.

Brito, D., Nataf, H.C., Cardin, P., Aubert, J., Masson, J., 2001. Ultrasonic Doppler velocimetry in liquid gallium. Experiments in Fluids 31, 653–663. doi:10.1007/s003480100312.

Bruno, R., Carbone, V., 2005. The solar wind as a turbulence laboratory. Living Reviews in Solar Physics 2. URL: `http://www.livingreviews.org/lrsp-2005-4`.

Buffett, B.A., 2003. A comparison of subgrid-scale models for large-eddy simulations of convection in the earth's core. Geophysical Journal International 153, 753–765. doi:10.1046/j.1365-246X.2003.01930.x.

Busse, F.H., 1970. Thermal instabilities in rapidly rotating systems. J. Fluid Mech. 44, 441–460.

Cardin, P., Olson, P., 2015. Experiments on core dynamics, in: Olson, P., Schubert, G. (Eds.), Treatise on Geophysics, Vol. 8 Core Dynamics, Elsevier B.V.. p. XXX.

Charbonneau, P., 2005. Dynamo Models of the Solar Cycle. Living Rev. Solar Phys. 2, [on line article] : cited [october 2, 2012] http://www.livingreviews.org/lrsp–2005–2.

Chen, Q., Jones, C.A., 2008. Similarity and dynamic similarity models for large-eddy simulations of a rotating convection-driven dynamo. Geophysical Journal International 172, 103–114. doi:10.1111/j.1365-246X.2007.03621.x.

Christensen, U., Aubert, J., 2006. Scaling properties of convection-driven dynamos in rotating spherical shells and application to planetary magnetic fields. Geophys. J. Int. 166, 97–114.

Christensen, U.R., Wicht, J., 2015. Numerical dynamo simulations, in: Olson, P., Schubert, G. (Eds.), Treatise on Geophysics, Vol. 8 Core Dynamics, Elsevier B.V.. p. XXX.

Davidson, P.A., 2013. Rapidly-rotating turbulence: an experimental perspective, in: Davidson, P.A., Kaneda, Y., Sreenivasan, K. (Eds.), Ten chapters in turbulence, Cambridge University Press. pp. 318–350.

Davidson, P.A., Staplehurst, P.J., Dalziel, S.B., 2006. On the evolution of eddies in a rapidly rotating system. Journal of Fluid Mechanics 557, 135–144. doi:10.1017/S0022112006009827.

Dritschel, D.G., McIntyre, M.E., 2008. Multiple jets as PV staircases: The Phillips effect and the resilience of eddy-transport barriers. Journal of the Atmospheric Sciences 65, 855–874. doi:10.1175/2007JAS2227.1.

Eymin, C., Hulot, G., 2005. On core surface flows inferred from satellite magnetic data. Phys. Earth Planet. Inter. 152, 200–220. doi:10.1016/j.pepi.2005.06.009.

Frisch, U., 1995. Turbulence: the legacy of A.N. Kolmogorov. Cambridge University Press.

Gailitis, A., Lielausis, O., Platacis, E., Dement'ev, S., Cifersons, A., Gerbeth, G., Gundrum, T., Stefani, F., Christen, M., Will, G., 2001. Magnetic Field Saturation in the Riga Dynamo Experiment. Phys. Rev. Lett. 86, 3024–3027. doi:10.1103/PhysRevLett.86.3024.

Giesecke, A., 2007. Anisotropic turbulence in weakly stratified rotating magnetoconvection. Geophys. J. Int. 171, 1017–1028. doi:10.1111/j.1365-246X.2007.03567.x.

Gillet, N., Jault, D., Canet, E., Fournier, A., 2010. Fast torsional waves and strong magnetic field within the earth's core. Nature 465, 74–77. doi:10.1038/nature09010.

Gillet, N., Schaeffer, N., Jault, D., 2011. Rationale and geophysical evidence for quasi-geostrophic rapid dynamics within the earth's outer core. Physics of the Earth and Planetary Interiors 187, 380–390. doi:10.1016/j.pepi.2012.03.006.

Gilman, P.A., Glatzmaier, G.A., 1981. Compressible convection in a rotating spherical shell. i - anelastic equations. II - a linear anelastic model. III - analytic model for compressible vorticity waves. The Astrophysical Journal Supplement Series 45, 335. doi:10.1086/190714.

Glatzmaier, G.A., Roberts, P.H., 1995. A three-dimensional self-consistent computer simulation of a geomagnetic field reversal. Nature 377, 203. doi:10.1038/377203a0.

Grote, E., Busse, F.H., Tilgner, A., 2000. Effects of hyperdiffusivities on dynamo simulations. Geophys. Res. Lett. 27, 2001–2004. doi:10.1029/1999GL011155.

Hogstrom, U., 1996. Review of some basic characteristics of the atmospheric surface layer. Boundary-Layer Meteorology 78, 215–246. doi:10.1007/BF00120937.

Holme, R., 2015. Large-scale flow in the core, in: Olson, P., Schubert, G. (Eds.), Treatise on Geophysics, Vol. 8 Core Dynamics, Elsevier B.V.. p. XXX.

Hulot, G., Eymin, C., Langlais, B., Mandea, M., Olsen, N., et al., 2002. Small-scale structure of the geodynamo inferred from Oersted and Magsat satellite data. Nature 416, 620–623.

Jault, D., 2008. Axial invariance of rapidly varying diffusionless motions in the Earth's core interior. Phys. Earth Planet. Inter. 166, 67–76.

Jault, D., Finlay, C., 2015. Waves in the core and mechanical core-mantle interactions, in: Olson, P., Schubert, G. (Eds.), Treatise on Geophysics, Vol. 8 Core Dynamics, Elsevier B.V.. p. XXX.

Jones, C., Soward, A., Mussa, A., 2000. The onset of thermal convection in a rapidly rotating sphere. J. Fluid Mech. 405, 157–179. doi:10.1017/S0022112099007235.

Kaneda, Y., Morishita, K., 2013. Small-scale statistics and structure of turbulence in the light of high resolution direct numerical simulation, in: Davidson, P.A., Kaneda, Y., Sreenivasan, K. (Eds.), Ten chapters in turbulence, Cambridge University Press. pp. 1–42.

Kelley, D., Triana, S., Zimmerman, D., Tilgner, A., Lathrop, D., 2007. Inertial waves driven by differential rotation in a planetary geometry. Geophys. Astrophys. Fluid Dyn. 101, 469–487. doi:10.1080/03091920701561907.

Kolmogorov, A., 1941a. Dissipation of energy in the locally isotropic turbulence. Dokl. Akad. Nauk. SSSR 32.

Kolmogorov, A., 1941b. The local structure of turbulence in incompressible viscous fluid for very large reynolds number. Dokl. Akad. Nauk. SSSR 30, 9–13.

Kolmogorov, A., 1962. A refinement of previous hypotheses concerning the local structure of turbulence in a viscous incompressible fluid at high reynolds number. J. Fluid Mech. 13, 82–85.

Kraichnan, R., Montgomery, D., 1980. Two-dimensional turbulence. Reports on Progress in Physics 43, 547–619. doi:10.1088/0034-4885/43/5/001.

Lathrop, D., Forest, C., 2011. Magnetic dynamos in the lab. Physics Today 64, 40–45.

Legras, B., Santangelo, P., Benzi, R., 1988. High-resolution numerical experiments for forced two-dimensional turbulence. Europhys. Lett. 5, 37–42. doi:10.1209/0295-5075/5/1/007.

Lo, T., L'vov, V., Pomyalov, A., Procaccia, I., 2005. Estimating von Karman's constant from homogeneous turbulence. Europhysics Letters 72, 943–949. doi:10.1209/epl/i2005-10323-8.

Loper, D., 2007. Turbulence and small-scale dynamics in the core, in: Olson, P., Schubert, G. (Eds.), Treatise on Geophysics, Vol. 8 Core Dynamics, Elsevier B.V.. pp. 187–206.

Matsui, H., Buffett, B.A., 2012. Large-eddy simulations of convection-driven dynamos using a dynamic scale-similarity model. Geophysical & Astrophysical Fluid Dynamics 106, 250–276. doi:10.1080/03091929.2011.590806.

Maximenko, N., Bang, B., Sasaki, H., 2005. Observational evidence of alternating zonal jets in the world ocean. Geophys. Res. Lett. 32. doi:10.1029/2005GL022728.

Moffatt, H., 1978. Magnetic Field Generation in Electrically Conducting Fluids. Cambridge University Press.

Moffatt, H.K., 1961. The amplification of a weak applied magnetic field by turbulence in fluids of moderate conductivity. J. Fluid Mech. 11, 625–635. doi:10.1017/S0022112061000779.

Monchaux, R., Berhanu, M., Bourgoin, M., Moulin, M., Odier, P., Pinton, J.F., Volk, R., Fauve, S., Mordant, N., Pétrélis, F., Chiffaudel, A., Daviaud, F., Dubrulle, B., Gasquet, C., Marié, L., Ravelet, F., 2007. Generation of a Magnetic Field by Dynamo Action in a Turbulent Flow of Liquid Sodium. Phys. Rev. Lett. 98, 044502–+. doi:10.1103/PhysRevLett.98.044502.

Nastrom, G., Gage, K., 1985. A climatology of atmospheric wavenumber spectra of wind and temperature observed by commercial aircraft. Journal of the Atmospheric Sciences 42, 950–960. doi:10.1175/1520-0469(1985)042¡0950:ACOAWS¿2.0.CO;2.

Nataf, H.C., Alboussière, T., Brito, D., Cardin, P., Gagnière, N., Jault, D., Schmitt, D., 2008. Rapidly rotating spherical Couette flow in a dipolar magnetic field: an experimental study of the mean axisymmetric flow. Phys. Earth Planet. Inter. 170, 60–72.

Nataf, H.C., Gagnière, N., 2008. On the peculiar nature of turbulence in planetary dynamos. C.R. Physique 9, 702–710. doi:10.1016/j.crhy.2008.07.009.

Nazarenko, S.V., Schekochihin, A.A., 2011. Critical balance in magnetohydrodynamic, rotating and stratified turbulence: towards a universal scaling conjecture. J. Fluid Mech. 677, 134–153. doi:10.1017/jfm.2011.67.

Niemela, J., Skrbek, L., Sreenivasan, K., Donnelly, R., 2000. Turbulent convection at very high Rayleigh numbers. Nature 404, 837–840. doi:10.1038/35009036.

Obukhov, A., 1941. Spectral energy distribution in a turbulent spectral energy distribution in a turbulent flow. Dokl. Akad. Nauk SSSR 32, 22–24.

Olson, P., 2015. Overview, in: Olson, P., Schubert, G. (Eds.), Treatise on Geophysics, Vol. 8 Core Dynamics, Elsevier B.V.. p. XXX.

Pais, M.A., Jault, D., 2008. Quasi-geostrophic flows responsible for the secular variation of the Earth's magnetic field. Geophys. J. Int. 173, 421–443. doi:10.1111/j.1365-246X.2008.03741.x.

Phillips, O., 1972. Turbulence in a strongly stratified fluidâ"is it unstable? Deep Sea Research and Oceanographic Abstracts 19, 79 – 81. doi:10.1016/0011-7471(72)90074-5.

Plunian, F., Stepanov, R., 2010. Cascades and dissipation ratio in rotating magnetohydrodynamic turbulence at low magnetic Prandtl number. Phys. Rev. E 82. doi:10.1103/PhysRevE.82.046311.

Plunian, F., Stepanov, R., Frick, P., 2013. Shell models of magnetohydrodynamic turbulence. Physics Reports 523, 1 – 60. doi:10.1016/j.physrep.2012.09.001.

Ponty, Y., Mininni, P.D., Montgomery, D.C., Pinton, J.F., Politano, H., Pouquet, A., 2005. Numerical study of dynamo action at low magnetic Prandtl numbers. Phys. Rev. Lett. 94, 164502+. doi:10.1103/PhysRevLett.94.164502.

Rieutord, M., Rincon, F., 2010. The Sun's supergranulation. Living Rev. Solar Phys. 7, [Online Article]: cited [october 2, 2012], http://www.livingreviews.org/lrsp–2010–2.

Rieutord, M., Triana, S.A., Zimmerman, D.S., Lathrop, D.P., 2012. Excitation of inertial modes in an experimental spherical Couette flow. Physical Review E 86. doi:10.1103/PhysRevE.86.026304.

Robert, R., Sommeria, J., 1991. Statistical equilibrium states for 2-dimensional flows. J. Fluid Mech. 229, 291–310. doi:10.1017/S0022112091003038.

Roberts, G.O., 1972. Dynamo action of fluid motions with two-dimensional periodicity. Phil. Trans. R. Soc. London, Ser. A 271, 411–454.

Roberts, P.H., 2015. Theory of the geodynamo, in: Olson, P., Schubert, G. (Eds.), Treatise on Geophysics, Vol. 8 Core Dynamics, Elsevier B.V.. p. XXX.

Sakuraba, A., Roberts, P.H., 2009. Generation of a strong magnetic field using uniform heat flux at the surface of the core. Nature Geoscience 2, 802–805. doi:10.1038/ngeo643.

Schmitt, D., Alboussière, T., Brito, D., Cardin, P., Gagnière, N., Jault, D., Nataf, H.C., 2008. Rotating spherical Couette flow in a dipolar magnetic field : Experimental study of magneto-inertial waves. J. Fluid Mech. 604, 175–197.

Schmitt, D., Cardin, P., La Rizza, P., Nataf, H.C., 2013. Magneto-Coriolis waves in a spherical Couette flow experiment. European J. Mech. B/Fluids 37, 10–22.

She, Z., Leveque, E., 1994. Universal scaling laws in fully-developed turbulence. Phys. Rev. Lett. 72, 336–339. doi:10.1103/PhysRevLett.72.336.

Soderlund, K.M., King, E.M., Aurnou, J.M., 2012. The influence of magnetic fields in planetary dynamo models. Earth Planet. Sci. Lett. 333-334, 9–20. doi:10.1016/j.epsl.2012.03.038.

Spence, E.J., Reuter, K., Forest, C.B., 2009. A spherical plasma dynamo experiment. Astrophys. J. 700, 470–478. doi:10.1088/0004-637X/700/1/470.

Steenbeck, M., Krause, F., Rädler, K., 1966. A calculation of the mean electromotive force in an electrically conducting fluid in turbulent motion, under the influence of Coriolis forces. Z. Naturforsch. A21.

Stefani, F., Gerbeth, G., Gundrum, T., Hollerbach, R., Priede, J.b.a., Rüdiger, G., Szklarski, J., 2009. Helical magnetorotational instability in a taylor-couette flow with strongly reduced ekman pumping. Phys. Rev. E 80, 066303. doi:10.1103/PhysRevE.80.066303.

Stieglitz, R., Müller, U., 2001. Experimental demonstration of a homogeneous two-scale dynamo. Phys. Fluids 13, 561–564. doi:10.1063/1.1331315.

StPierre, M., 1996. On the local nature of turbulence in earth's outer core. Geophys. Astrophys. Fluid Dyn. 83, 293–306.

Swinbank, W.C., 1951. The measurement of vertical transfer of heat and water vapour and momentum in the lower atmosphere with some results. J. Meteorol. 8, 135–145.

Tobias, S., Cattaneo, F., Boldyrev, S., 2013. MHD dynamos and turbulence, in: Davidson, P.A., Kaneda, Y., Sreenivasan, K. (Eds.), Ten chapters in turbulence, Cambridge University Press. pp. 351–404.

Vasavada, A., Showman, A., 2005. Jovian atmospheric dynamics: an update after Galileo and Cassini. Reports on Progress in Physics 68, 1935–1996. doi:10.1088/0034-4885/68/8/R06.

Verhille, G., Plihon, N., Bourgoin, M., Odier, P., Pinton, J.F., 2010. Laboratory Dynamo Experiments. Space Science Reviews 152, 543–564. doi:10.1007/s11214-009-9546-1.

Westerweel, J., Elsinga, G.E., Adrian, R.J., 2013. Particle image velocimetry for complex and turbulent flows. Annual Review of Fluid Mechanics 45, 409–436. doi:10.1146/annurev-fluid-120710-101204.

Xu, H., Bourgoin, M., Ouellette, N., Bodenschatz, E., 2006. High order Lagrangian velocity statistics in turbulence. Phys. Rev. Lett. 96. doi:10.1103/PhysRevLett.96.024503.